SASOR 2012

4th Southern African Conference on Rheology

10-11 September 2012

Conference Proceedings

Edited by
Veruscha Fester

SASOR SOUTHERN AFRICAN SOCIETY OF RHEOLOGY

www.sasor.co.za

4th Southern African Conference on Rheology

SASOR 2012

Cape Town
South Africa
10 – 11 September 2012

Programme & Abstracts

Organising Committee

Prof I Masalova
Prof V Fester
Prof R Haldenwang
Dr S Woudberg
Ms F Qondani

Technical Committee

Prof I Masalova
Prof P Slatter
Dr S Woudberg

Welcome

Welcome to the 4th Southern African Conference on Rheology, SASOR 2012. We held our first conference in 2006. Our second conference in 2008 came soon after the International Committee on Rheology's meeting in Monterey in August 2008, where we were elected to full membership of this international body. This represents full recognition of our young society, and we have been assigned to the European sector of the ICR. Our third conference SASAR 2010 was well attended by the international rheological community with speakers from France, Italy, Sweden and the USA.

This year, however, we are very pleased to have the same number of local speakers from industry and academia as our international speakers, showing that the interest is growing in South Africa.

SASOR 2012 will consist of plenary lectures and oral presentations. The really valuable discussions, debate and interactions are in reality up to you – so please participate as freely as you are able. We hope that you will find the conference stimulating.

We wish to express our gratitude to the individuals and organizations that have contributed to the success of the conference.

Prof Irina Masalova
SASOR 2012 Chair

Programme

Monday 10 September 2012			Page
08:30		Registration : Coffee/Tea	
09:15		**Opening: President of SASOR**	
		Chairperson: *Irina Masalova*	
09h30	P1	**Plenary: Prof C Gallegos** **Rheological Aspects of Swallowing and Dysphagia** *President of European Rheology Society,* *Vice-President. Head I&D Centre "Complex Formulations" Clinical Nutrition & Pharmaceuticals. Science, Production & Technology Fresenius Kabi Deutschland GmbH*	8
10:20		Questions	
10:35	S1	**Effect of multi-walled carbon nanotubes concentration in oil phase on properties of highly concentrated water-in-oil emulsions** E Kharatyran I Masalova* °*AEL Mining Services, AEL Research ans Development Department, Modderfontein,* * *Research Rheology Laboratory, Engineering Faculty, Cape Peninsula University of Technology*	20
10:55		Questions	
11:00		**Coffee/Tea**	
		Chairperson: *Jeffrey Giacomin*	
11:30	P2	**Plenary: Prof G Fuller** **Interfacial rheology of biofilms associated with infectious disease** *Fletcher-Jones Professor of Chemical Engineering at Stanford University, USA*	10
12:20		Questions	
12:35	S2	**Using fumed silica nano particles in combination with SMO conventional surfactant to stabilize w/o highly concentrated emulsion (explosive type): Effect of particle hydrophobicity on rheological properties.** N Tshilumbu, *I Masalova *Research Rheology Laboratory, Engineering Faculty, Cape Peninsula University of Technology, South Africa*	26
12:55		Questions	
12:50		**Promotion: Gold Sponsor: AEL**	
13:00		**Lunch**	
		Chairperson: *Rainer Haldenwang*	
14:00	P3	**Plenary: Dr P Fischer** **Flow instabilities in wormlike micellar solution** *Institute of Food Sciences and Nutrition, ETH, Zurich*	11
14:50		Questions	
15:05	S3	**Rheology of maize starch modified with lipids** MN Emmambux, OC Wokadala *Department of Food Science, University of Pretoria*	35
15:25		Questions	
15:40		**SASOR AGM**	
18:30		**Conference Dinner**	

Tuesday 11 September 2012			Page
09:00		Registration : Coffee/Tea	
		Chairperson: *Gerry Fuller*	
09h30 10:20	P4	**Plenary: Prof A Jeffrey Giacomin** **Viscous Heating in Large Amplitude Oscillatory Shear** *Chair, Rheology Research Center, Professor of Mechanical Engineering and Polymer Engineering Center, University of Wisconsin , Madison* Questions	
10:25 10:45	S4	**Methodology for coupled cfd-dem modelling of particulate suspension rheology** EM Smuts *, DA Deglon *, CJ Meyer ° **Minerals to Metals, Chemical Engineering Department, University of Cape Town* *°Department of Mechanical and Mechatronic Engineering, University of Stellenbosch* Questions	39
10:50		**Coffee/Tea**	
		Chairperson: *Sonja Woudberg*	
11:20 12:10	P5	**Plenary: Prof P Slatter** **Rheological Characterisation Using Free Surface Flows** *Professor of Rheology and Fluid Engineering, Director: Rheology and Materials Processing Centre School of Civil, Environmental and Chemical Engineering, RMIT University, Melbourne, Australia.* Questions	14
12:25 12:45	S5	**A comparison of 150mm pipeloop data with rotational viscometer test methods** B Zengeni, R Malloch, F van Sittert *Paterson & Cooke Consulting Engineers (Pty) Ltd, Cape Town* Questions	45
12:50		**CONFERENCE CLOSING**	
13:00		**Lunch**	

Street Map

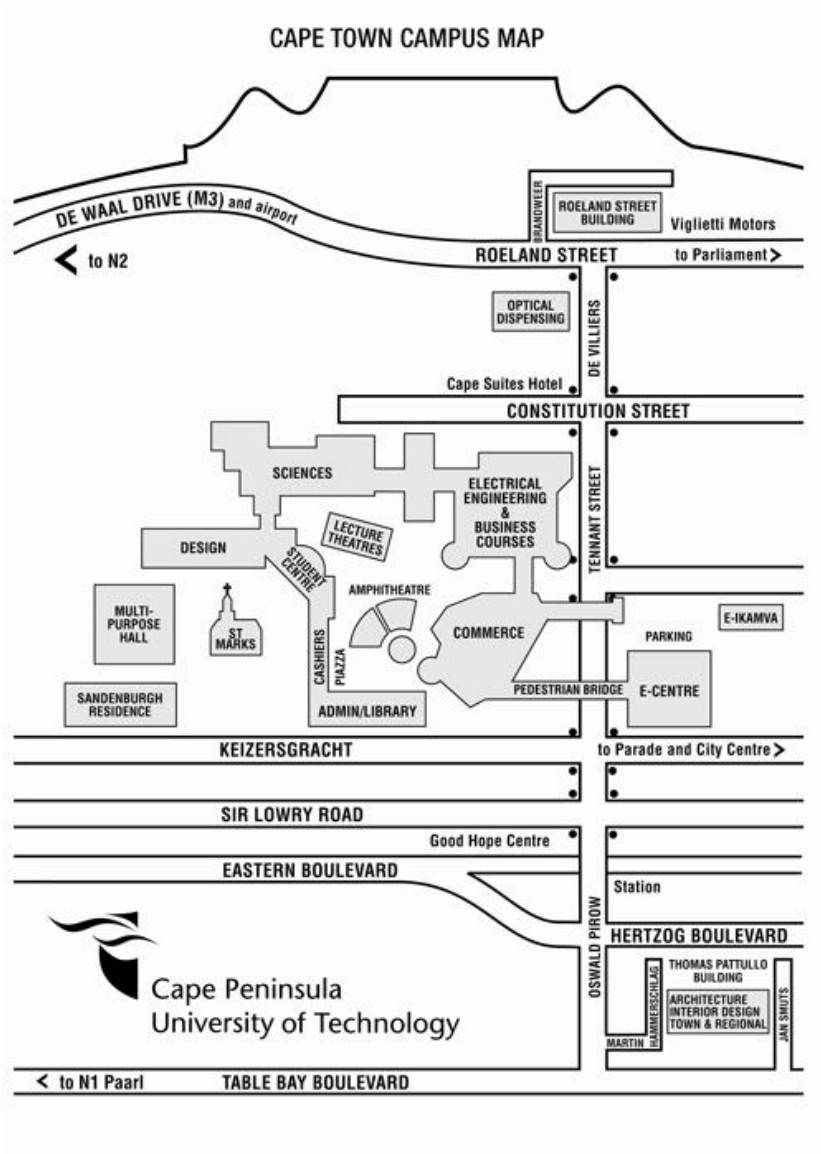
CAPE TOWN CAMPUS MAP
DE WAAL DRIVE (M3) and airport
to N2
BRANDWEER
ROELAND STREET BUILDING
Viglietti Motors
ROELAND STREET
to Parliament
OPTICAL DISPENSING
DE VILLIERS
Cape Suites Hotel
CONSTITUTION STREET
SCIENCES
ELECTRICAL ENGINEERING & BUSINESS COURSES
TENNANT STREET
LECTURE THEATRES
DESIGN
STUDENT CENTRE
AMPHITHEATRE
MULTI-PURPOSE HALL
ST MARKS
CASHIERS
PIAZZA
COMMERCE
E-IKAMVA
PARKING
SANDENBURGH RESIDENCE
ADMIN/LIBRARY
PEDESTRIAN BRIDGE
E-CENTRE
KEIZERSGRACHT
to Parade and City Centre
SIR LOWRY ROAD
Good Hope Centre
EASTERN BOULEVARD
Station
HERTZOG BOULEVARD
OSWALD PIROW
THOMAS PATTULLO BUILDING
ARCHITECTURE INTERIOR DESIGN TOWN & REGIONAL
HAMMERSCHLAG
MARTIN
JAN SMUTS
Cape Peninsula University of Technology
to N1 Paarl
TABLE BAY BOULEVARD

Campus Plan

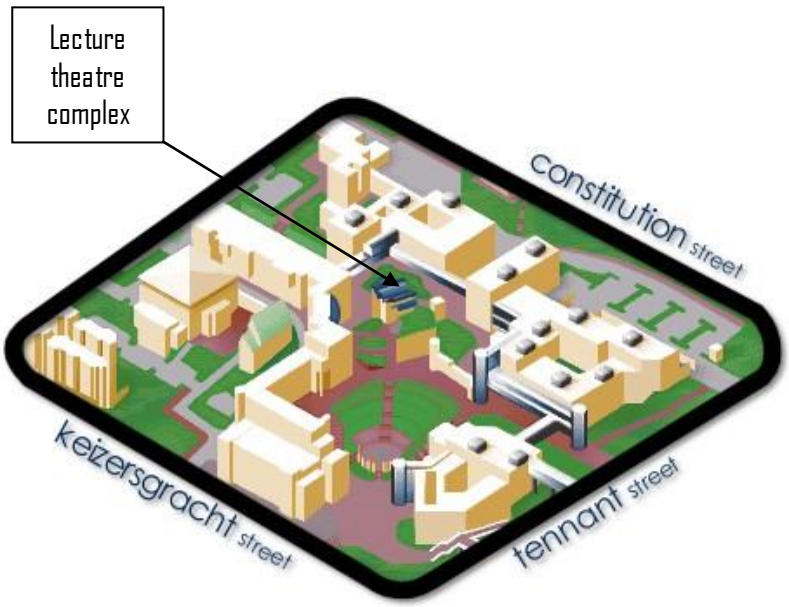

Conference Area

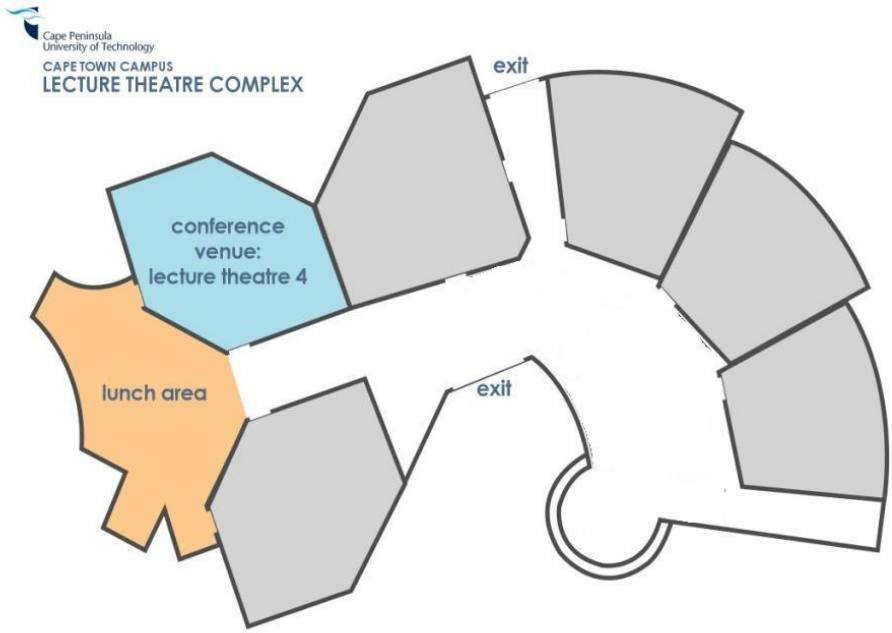

RHEOLOGICAL ASPECTS OF SWALLOWING AND DYSPHAGIA

Crispulo Gallegos[1,2], Gabriel Ascanio[3] and Edmundo Brito-de la Fuente[4]

[1]I&D Centre Complex Formulations. Fresenius Kabi Deutschland GmbH. Daimlerstrasse, Bad Homburg (Germany)
[2]Departamento de Ingeniería Química. Universidad de Huelva. 21071 Huelva (Spain)
[3]Centro de Ciencias Aplicadas y Desarrollo Tecnológico. UNAM. Mexico DF (Mexico)
[4]I&D Clinical Nutrition & Pharmaceuticals. Fresenius Kabi Deutschland GmbH. Borkenberg Oberursel (Germany)

Dysphagia, or abnormal swallowing of foods and/or liquids, is a consequence of neurological diseases, several forms of cancer, or stroke. Dysphagia is usually related to a reduced oral intake that easily leads to malnutrition and dehydration.

The main objective of dysphagia assessment is to avoid food aspiration (food to enter into the airway passing the vocal folds), because this may lead to pneumonia. Aspiration and penetration, this last defined as the passage of materials into the larynx, depend on clinical status as well as food/liquid flow properties and bolus volume.

Management of dysphagia is commonly done by the prescription of texture-controlled diets. Texture or consistency modification of liquids or solids is commonly done by using food thickeners in powder form. One drawback of using powdered thickeners is the control of consistency or flow properties in the final product. An alternative to this practice is the use of prescribed ready-to-use (RTU) oral nutritional supplements (ONS) specially designed for the nutritional support at different stages of dysphagia. These ONS may represent several advantages from a nutritional point of view, because they are specially designed for complete nutrition, in addition to a controlled consistency or texture.

The rationale behind altering or modifying the consistency of foods and/or drinks is to change the rate at which food is transported through the pharynx and, thus, to reduce the risk of aspiration. Although the most appropriate modification of food consistencies should follow from a clear assessment of the swallowing problem, quite often health care professionals relay on National guidelines for the dietary management of dysphagia patients. For instance, the National Dysphagia Diet (NDD, American Dietetic Association, USA) proposed different terms for liquids and correlating viscosity ranges, at 25°C and a single shear rate of 50 s^{-1}: (1) Thin: 1-50 cP; (2) Nectar-like: 51-350 cP; (3) Honey-like: 351-1750 cP; (4) Spoon-thick: >1750 cP. There is no scientific evidence or rationale given by NDD on the temperature and shear rate chosen for this scale. On the other hand, these scales only consider viscous properties; elasticity is not even mentioned.

In summary, most of the available information regarding the rheological properties of ready-to-use diets/foods used for dysphagia management is mainly focused on viscosity. However, the need for more comprehensive rheological information on ready-to-use products for dysphagic patients has been highlighted by different authors.

The aim of this lecture is to present an overview on recent advances concerning fluid dynamics analysis of the swallowing process and the role of rheology in product design for dysphagia nutritional support.

The kinematic/dynamic analysis of dysphagia demonstrates that bolus transit velocity is significantly higher for the pharyngeal than for the esophageal phase of the swallowing process. In general, the shear rate range during this process varies from 1 to 1000 s^{-1}. However, most of the literature is focused on shear flow, whilst little attention has been paid to the role of elongational flows in dysphagia.

Rheology and swallowing are also connected at the diagnosis level. Thus, the swallowing process can be visualized using videoradiography by employing either ready-to-use commercial contrast medium or by mixing food with barium sulphate, making it radiopaque. Aiming to close the gap with videofluoroscopic fluids, a rheological similarity approach will be presented for the design of new products for the nutritional management of dysphagic patients.

INTERFACIAL RHEOLOGY OF BIOFILMS ASSOCIATED WITH INFECTIOUS DISEASE

Cynthia Wu, Ji Youn Lim, Lynette Cegelski, Gerald G. Fuller

Departments of Chemical Engineering and Chemistry
Stanford University Stanford, CA 94305-5025

Bacterial biofilms are complex multi-cellular assemblies characterized by a heterogeneous extracellular polymeric matrix that have emerged as hallmarks of persistent infectious diseases. New approaches and quantitative data are needed to examine biofilm composition and architecture and to correlate these with the mechanical and physicochemical properties that relate to function. We performed a panel of interfacial rheological measurements during biofilm formation at the air-liquid interface by the E. coli strain, UTI89, noted for its importance in studies of urinary tract infection and for its assembly of functional amyloid fibers termed curli. Brewster-angle microscopy and measurements of the surface elasticity (G_s') and stress-strain response provided sensitive and quantitative parameters that revealed distinct stages during bacterial colonization, aggregation, and eventual formation of a pellicle at the air-liquid interface. Pellicles formed under conditions that upregulate curli production exhibited an increase in strength and viscoelastic properties as well as a greater ability to recover from stress-strain perturbation. The results suggest that curli, as hydrophobic extracellular amyloid fibers, enhance the strength, viscoelasticity, and resistance to strain of E. coli biofilms formed at the air-liquid interface.

FLOW INSTABILITIES IN WORMLIKE MICELLAR SOLUTION

Viviane Lutz-Bueno, Joachim Kohlbrecher, Peter Fischer

Institute of Food, Nutrition and Health, Schmelzbergstrasse 9, 8092 Zurich, Switzerland
Laboratory for Neutron Scattering, Paul-Scherrer Institute, 5232 Villigen, Switzerland

Surfactants are amphiphilic molecules, which can self-assemble into aggregates of different sizes and shapes like spherical, cylindrical, and wormlike micelles as well as lamellae and vesicles in aqueous media. Diluted and semi-diluted solutions of wormlike micelles are viscoelastic and exhibit very rich rheological behavior with the formation of shear-induced structures (SIS) [1-2]. Beside a brief review on the experimental phenomena and theoretical efforts we will focus on the non-linear rheological properties of equimolar surfactant solutions under shear and contraction flow conditions [3-6]. Rheological and optical techniques such as flow visualization, rheo-SALS, and rheo-SANS are used to picture the structural properties in stress and strain driven environments. So the formation of alternating shear bands for semi-diluted solution can be analyzed in a time-resolved SANS set-up coupled with high-speed video imaging.

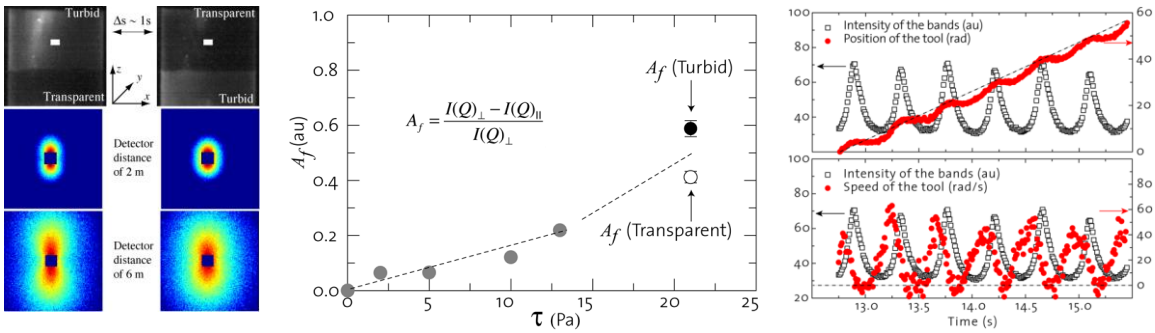

Figure 1 Time resolved SANS pattern (left) and anisotropy factor for the shear-thickening turbid and clear band (middle). The optical analysis of the rotational motion of the Couette tool and the appearance of the turbid band reveals that the more aligned state is also the more viscous state (right).

The transient behavior of the structure factor indicates a cyclic formation and destruction of strongly aligned wormlike micelles leading to macroscopically observed rate oscillations [7]. The surfactant solution never reaches equilibrium situation due to the feedback loop between applied stress and rate controlled structure formation see Figure 1.

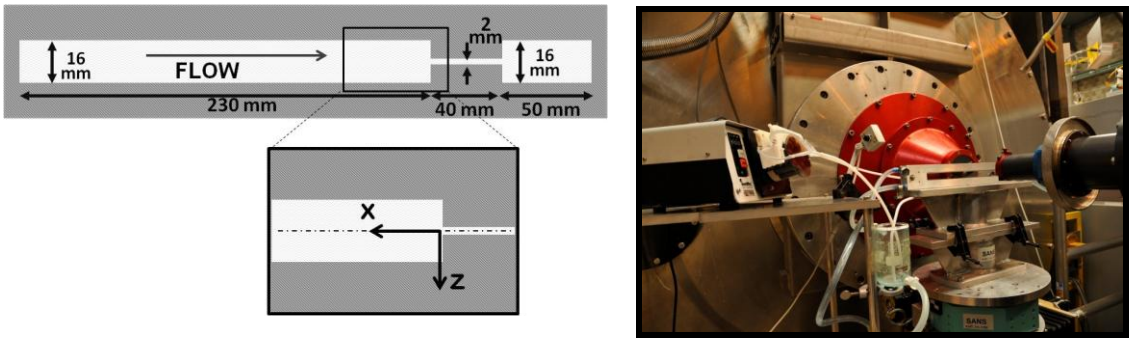

Figure 2 (left) Dimensions of the planar flow contraction geometry. Detail: SANS scanned area. (right) Set-up of the SANS experiment with the flow cell and the tubing loop.

A similar phenomenon can be observed in contraction flow for diluted surfactant solutions. Here the surfactant solution not only builds up a transient entry flow regime but additionally exhibits a strong upstream-oriented jet. Figure 2 shows a schematic of the contraction flow cell and the entire neutron scattering set-up that was used to investigate the spatio-transient orientation behavior. The alignment of the micellar solution in the entrance as well as in the up-stream region is analyzed in terms of the anisotropy of the SANS scattering patterns as depicted in Figure 3.

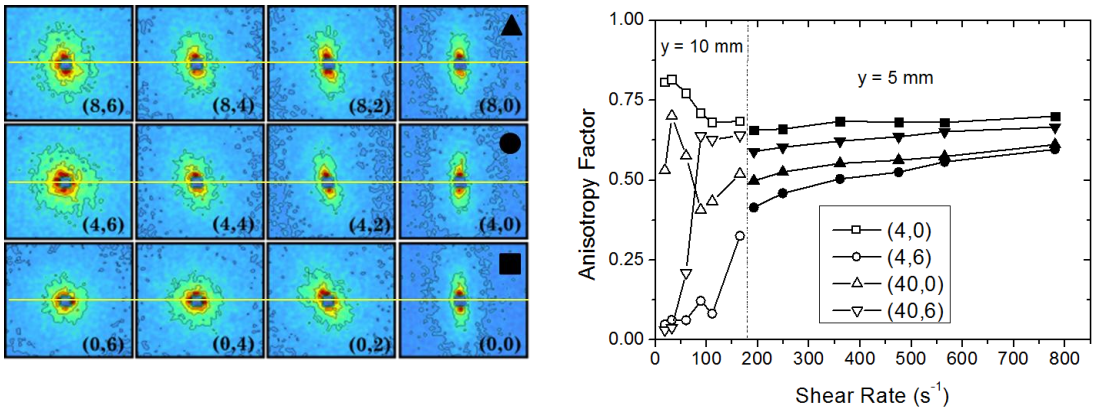

Figure 3 (left) Scattering patterns at different (x, z) positions along the flow cell (y = 1mm). (right) Anisotropy factor for different flow rates and (x, z) positions under different y-confinement (flow cell height).

Sectorial alignment can be enhanced not only by the flow rate but also under increasing confinement of the micellar solution (reducing the flow cell height). Even though micelles have dimensions in nm to μm range, geometrical confinement in the mm range influence their orientation under flow as already reported earlier [5]. The increase of the micellar length in the upstream orientation suggest that the strong jetting flow is self-supporting and can therefore move up-stream by simply growing from the surrounding isotropic material. As driving mechanism the already

introduced feedback loop between applied stress and flow rate that controls the structure formation is proposed.

REFERENCES

[1] W.M. Gelbart, A. Ben-Shaul, D. Roux: Micelles, Membranes, Microemulsions and Monolayers, Springer, Berlin (1994).
[2] J.-F. Berret: Rheology of Wormlike Micelles: Equilibrium Properties and Shear Banding Transitions, in Molecular Gels - Part 6, Springer, Berlin (2006).
[3] E.K. Wheeler, P. Fischer, G.G. Fuller: Time-periodic flow induced structures and instabilities in a viscoelastic surfactant solution, J. Non-Newton. Fluid Mech. 75 (1998) 193.
[4] P. Fischer, E.K. Wheeler, G.G. Fuller: Shear-Banding structure orientated in the vorticity direction observed for equimolar micellar solution, Rheol. Acta 41 (2002) 35.
[5] V. Herle, P. Fischer, E.J. Windhab: Stress driven shear bands and the effect of confinement on their structures - a rheological, flow visualization and rheo-SALS study, Langmuir 21 (2005) 9051.
[6] V. Lutz-Bueno, J. Kohlbrecher, P. Fischer: Shear thickening, temporal shear oscillations and degradation of dilute equimolar CTAB/NaSal wormlike solutions, submitted.
[7] V. Herle, J. Kohlbrecher, B. Pfister, P. Fischer, E.J. Windhab: Alternating vorticity bands in a solution of wormlike micelles, Phys. Rev. Lett. 99 (2007) 158302.

RHEOLOGICAL CHARACTERISATION USING FREE SURFACE FLOWS

Prof Paul Slatter

Professor of Rheology and Fluid Engineering
Director: Rheology and Materials Processing Centre
School of Civil, Environmental and Chemical Engineering
RMIT University, Melbourne, Australia.
Email: paul.slatter@rmit.edu.au

INTRODUCTION

The sheet flow of viscous material is of critical importance in many industrial settings. Our previous studies have shown that a sheet flow diagram could be constructed, and that these flows could be scaled for engineering design purposes in a manner similar to the approach of Metzner and Reed for tube flow. However, many unresolved issues remain for the rheometrical measurement and flow behaviour analyses of sheet flow. Arguably, the most acute of these are the application to viscoplastic material and the concomitant location of the Laminar/Turbulent transition. The objective of this paper is to develop and evaluate this approach for the flow behaviour analyses, rheological characterisation, and prediction of the Laminar/Turbulent transition for viscoplastic sheet flows. Using experimental data, it is shown that this approach works well for the analysis of viscoplastic materials.

THEORY AND LITERATURE

For sheet flows, the shear stress τ increases linearly from zero at the free surface to a maximum at the wall shear stress τ_0 at depth H. The shear stress distribution is as indicated in Figure 1:

$$\tau = \rho g h \sin\alpha \qquad (1)$$

Where:
τ = the shear stress at depth h (Pa).
ρ = the fluid density (kg/m^3).
g = gravitational acceleration (m/s^2).
h = the depth of fluid in the sheet (m).
α = inclination (degrees).
The shear stress distribution is shown in Figure 1.

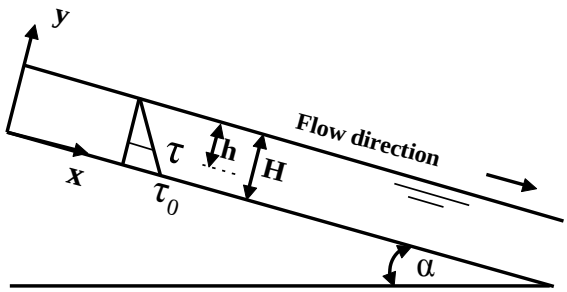

Figure 1 Shear stress distribution for sheet flow (Chow, 1959)

for laminar Newtonian sheet flow the volumetric flow rate relationship is obtained by integrating Equation (1) over the flow depth (Chow, 1959):

$$Q = \frac{H^2 \tau_0}{3\mu} \qquad (2)$$

Where:
Q = volumetric flow rate *per unit channel width* ($m^3/s/m$).
H = fluid height (m).
τ_0 = wall shear stress (Pa).
μ = dynamic viscosity (Pa.s).

Expressed in terms of the mean velocity V, we have:

$$V = \frac{Q}{H} = \frac{H\tau_0}{3\mu} \qquad (3)$$

where:
V = mean velocity (m/s).
Thus, for a Newtonian fluid, the wall shear stress and the wall shear rate the relationship is as follows:

$$\tau_0 = \mu \frac{3V}{H} = \mu \dot{\gamma}_0 \qquad (4)$$

therefore:

$$\dot{\gamma}_0 = \frac{3V}{H} \qquad (5)$$

which gives us the bulk sheet flow shear rate for sheet flow as $3V/H$.
The wall shear stress for sheet flow is:

$$\tau_0 = \rho g H \sin\alpha \qquad (6)$$

Laminar sheet flow can therefore be represented and analysed as a unique relationship between wall shear stress τ_0 and bulk shear rate *3V/H*, as is customarily done for pipe flow.
The sheet flow analysis for a general time independent non-Newtonian fluid can be obtained (Slatter et al., 2010) in terms of the bulk shear rate as:

$$\frac{3V}{H} = \frac{3}{\tau_0^2}\int_0^{\tau_0} \tau\dot{\gamma}(\tau)d\tau \qquad (7)$$

By analogy with tube flow, one can introduce the apparent sheet flow behaviour index n_*' defined as the slope of the logarithmic plot of wall shear stress τ_0 versus bulk shear rate *3V/H* (Slatter et al., 2010). Finally, the shear rate at the wall is expressed in terms of the bulk shear rate (*3V/H*) as (Slatter et al., 2010):

$$\dot{\gamma}_0 = \frac{3V}{H}\left(\frac{2n_*' + 1}{3n_*'}\right) \qquad (8)$$

Table 1 expresses the analogies between the proposed sheet flow analysis and that of the Rabinowitsch and Mooney approach for tube flow.

Table 1 Comparison of key elements of the rheometric analysis of tube to sheet flow (Slatter et al., 2010)

	Bulk Shear Rate	Wall Shear Stress	R-M Factor
Tube Flow	$\frac{8V}{D}$	$\frac{D\Delta p}{4L}$	$\frac{3n'+1}{4n'}$
Sheet Flow	$\frac{3V}{H}$	$\rho g H \sin\alpha$	$\frac{2n_*'+1}{3n_*'}$

The apparent sheet flow behaviour index n_*' has been defined in terms of a power law relationship between the wall shear stress τ_0 and the bulk shear rate *3V/H*. Having established a power law relationship, we can define an apparent sheet flow fluid consistency index K_*' After the method of Metzner and Reed (1955) as:

$$K_*' = \frac{\tau_0}{\left(\frac{3V}{H}\right)^{n_*'}} \; . \qquad (9)$$

This leads to the fundamentally important laminar flow design equation for sheet flow as:

$$\tau_0 = K_*'\left(\frac{3V}{H}\right)^{n_*'} \; . \qquad (10)$$

We can now define a new Reynolds number for sheet flow after the Newtonian paradigm:

$$\mathrm{Re}_4 = \frac{8\rho V^2}{\tau_0} \quad . \qquad (11)$$

Slatter et al. (2011) have shown that this approach works well for a power law fluid. In particular they have shown that for a power law material, the laminar/turblent transition can be predicted using a transition criterion of Re_4=700. In this paper we apply this same approach to a viscoplastic material.
As noted above, the apparent sheet flow behaviour index n'_* has been defined in terms of a power law relationship between the wall shear stress τ_0 and the bulk shear rate *3V/H*, and will be constant for a power law material. However, this will not hold for a viscoplastic material, and the apparent sheet flow behaviour index n'_* will need to be evaluated as a tangent at the relevant wall shear stress.

RESULTS

The previously published results for a kaolin slurry will be used for illustrative purposes in this paper (Haldenwang and Slatter, 2006).

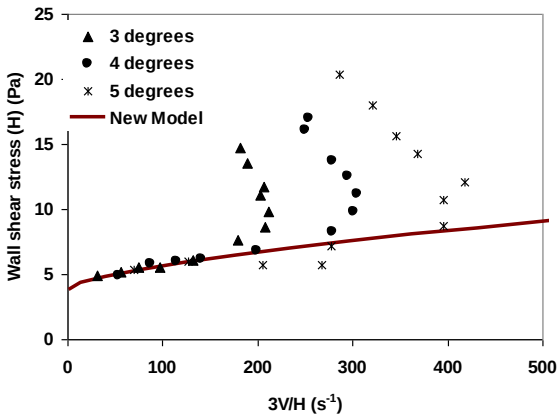

Figure 2: Sheet flow diagram for the kaolin slurry

Figure 2 shows the sheet flow data for the kaolin slurry, together with the new laminar sheet flow modelling approach as proposed by Slatter et al. (2011).

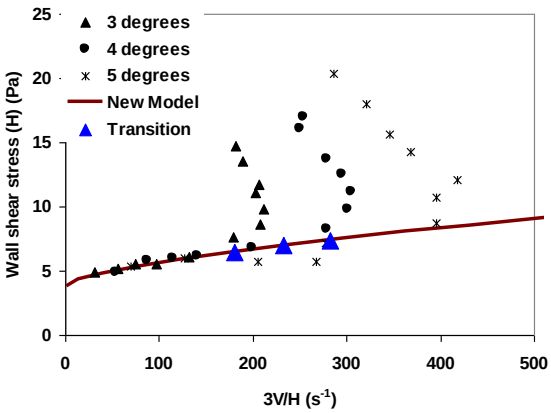

Figure 3: Sheet flow diagram for the kaolin slurry, showing predicted laminar/turbulent transition points

Figure 3 shows the predicted laminar/turbulent transition points against the actual sheet flow data for the kaolin slurry.

DISCUSSION

Figure 2 and Figure 3 show that the approach has considerable merit for the viscoplastic material portrayed. However, it could be argued that the flow behaviour predictions for both the laminar flow and the laminar/turbulent transition point are not as good for the 5° slope as they are for the 3° and 4° slopes. The reason for this may be Froude Number effects, due to the intereference of tranquil/shooting transition flow surface wave effects with the laminar/turbulent flow transition phenomenon.
The effect of Froude number and tranquil/shooting transition flow surface wave effects should be investigated further, especially for viscoplastic fluids where the presence of the yield stress will have a damping influence.
Figure 2 and Figure 3 also reveal another somewhat puzzling feature. The turbulent flow regions for each slope assume a negative gradient after the laminar/turbulent transition. There are thus two wall shear stress values applicable to each 3V/H value. This would appear to be counter-intuitive, and requires further investigation.

CONCLUSIONS

The previously developed approach (Slatter et al. 2010), which was shown to be successful for power law fluids (Slatter et al. 2011), has now been extended to viscoplastic fluids. The approach has been validated against experimental viscoplastic data, and found to have significant merit in this case. Issues requiring further work have been identified and discussed.

REFERENCES

1. Chow, V.T. (1959) Open Channel Hydraulics, McGraw-Hill Book Co-Singapore.
2. Slatter, P.T., Haldenwang, R. and Chhabra, R.P. (2010) The Sheet Flow Viscometer, Hydrotransport 18, in Proceedings 18th International Conference on the Hydraulic Transport of Solids, BHR Group, Rio de Janeiro, 22–24 September.
3. Metzner, A.B. and Reed, J.C. (1955) Flow of non-Newtonian fluids - correlation of the laminar, transition and turbulent flow regions, AIChE Journal, Vol. 1, No. 4.
4. Slatter PT Haldenwang R and Chhabra RP (2011); The laminar/turbulent transition for paste sheet flow, Paste 2011, R.J.Jewel and A.B.Fourie (eds); 14th International Seminar on Paste and Thickened Tailings, Perth, Australia;5-7 April 2011. ISBN 978-0-9806154-3-2, pp381-388.
5. Haldenwang R, and Slatter P T, (2006), Experimental procedure and database for non-Newtonian open channel flow, Journal of Hydraulic Research, Vol. 44, No. 2, pp. 283-287.

EFFECT OF MULTI-WALLED CARBON NANOTUBES CONCENTRATION IN OIL PHASE ON PROPERTIES OF HIGHLY CONCENTRATED WATER-IN-OIL EMULSIONS

Ellina Kharatyan°, Irina Masalova*

°AEL Mining Services, AEL Research and Development Department, Andreer Road, Pinelands Office Park, Building N7 Pinelands, Modderfontein, E-mail: Ellina.Kharatyan@aelms.com
* Research Rheology Laboratory, Engineering Faculty,Cape Peninsula University of Technology (CPUT), P.O.Box 8000, Cape Town, South Africa, Email: masalovai@cput.ac.za

INTRODUCTION

In spite of the fact that carbon nanotubes were discovered only 20 years ago [1, 2], for this rather short period of time they have turned from exotic objects to standard technological items and one can find a great number of attempts to find the best ways of their application in periodicals and patents, as well as multidisciplinary investigations of their structure and properties. Now nanotubes is a genral name for a family of materials: single walled carbon nanotbes, multiwalled carbon nanotubes (MWCNT) and modified nanotubes. Nanotubes are widely used in different applications [1,2], but one of the most interesting utilizations of carbon nanotubes is in their use as a stabilizer in colloidal dispersions. The application of nano-tubes as a surfactant to stabilize the water-oil interface can be treated as so-called Pickering emulsions [3-5]. Since carbon nanotubes are not soluble in water nor in oil they are able to assemble at the aqueous-oil interface forming a smooth, ultra thin film of 3-8 nm thickness [6]. Moreover, nanotubes, as any nano- or micro-sized objects, are prone to aggregation, forming networks with fractal-like structures.
The necessary effect of the application of nanotubes can be achieved only through the optimization of a morphological structure. So it is crucial to create good dispersion that can be made possible by the chemical treatment of nano-particles and the addition of a surfactant [7].
The goal of this work is to consider the possibility of using nanotubes (MWCNT) as a surfactant or co-surfactant to stabilize water-in-oil (w/o) highly concentrated emulsions. One of the goals of the work was the replacement of the conventional emulsifier mixtures that are used for such emulsions, with nanotubes in combination with cheap classic surfactants such as sorbitan monooleate (SMO).

MATERIALS AND METHODS

The water-in-oil highly concentrated emulsions were the main object of the investigation. Such emulsions were described in detail in [8-12]. So, only a brief characterization of emulsions will be given here. The dispersed phase droplets consist of 80% water solution of ammonium nitrate, the ammonium nitrate dissolution

temperature is typically greater than 60oC; all the experiments were carried out at lower (ambient) temperatures, so in other words the dispersed phase is thermodynamically unstable – super-cooled solution. The upper limit of the internal phase reached was app. 94 % by mass. The emulsion density is 1.4 g/cm3. The stabilization of emulsion reached by using MWCNT only or combination of MWCNT with SMO. The concentration of the latter was 5% in oil phase. MWCNT were supplied by Nanostructured & Amorphous Materials, Inc. and used as received. Three types of MWCNT were used:
Pristine MWCNT, with the content of the basic component of 88%; an outside diameter of 10-30 nm, inside diameter of 5-10 nm; length of 10-30 μm; specific surface area of 100-130 m2/g; residual content of Al2O3 <9% and NiO <3%.

- Functionalized MWCNT containing 2.36-2.60 wt % of -OH groups.
- Functionalized MWCNT containing 1.47-1.63 w% of -COOH groups.

As a general rule, MWCNT suspensions that are used for applications as Pickering-type surfactants are prepared by dispersing them in an aqueous phase (see, e.g. [16]). We used suspensions of MWCNT in an oil phase. The concentration of MWCNT varied from 0.1 to 2-wt%. The dispergator Silverson L4RT was used for dispersing MWCNT in the oil phase.
The MWCNT suspension was mixed with an aqueous phase by means of a Hobart mixer and a standard procedure for preparing w/o emulsions. The time of mixing tmix plays a crucial role, because the average size of the aqueous droplets depends on tmix. The dependencies of the degree of refinement on tmix are quite similar for all compositions under study. Our target average droplet size of emulsion was in the order of 10 μm, and it was reached at a tmix equal to app. 3-4 min and in the case of SMO stabilized emulsions (without MWCNT), the manufacturing tmix was increased to 5 min. So, this time is enough to form an interface stabilizing layer containing MWCNT particles.

RESULTS AND DISCUSSION

Rheology

The first aspect of the study is the modification of the oil properties as a function of MWCNT concentration. It is interesting to mention that the oil phase with no additives is close to the behaviour of a Newtonian liquid (Fig. 1) and with the introduction of nano-tubes structure build-up in the oil phase was observed.
Based on Fig. 2 it is clear that the increase in the strength of the structure formed due to the presence of MWCNT is most pronounced up to the nano-tube concentration of 1%. With a further increase of MWCNT concentration in the oil, the effect is less expressed. This can be related to the non-uniform dispersion of nano-tubes or in other words, by the formation of clusters (aggregates).

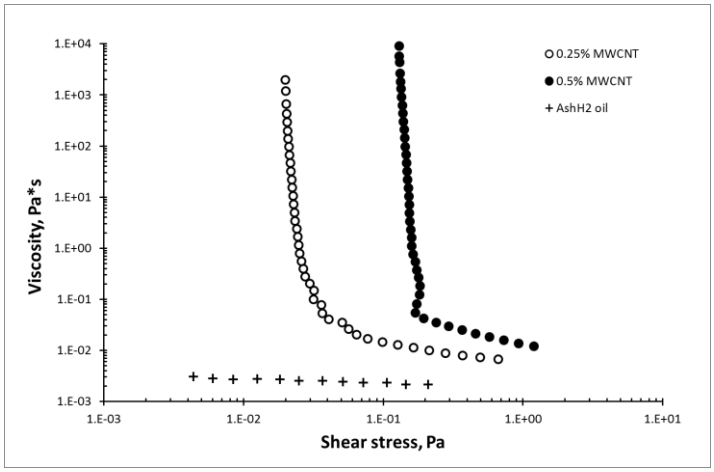

Figure 1 Flow properties of a continuous oil phase: crosses - oil itself; circles – with addition of MWCNT

The structure build-up demonstrated by the appearance, followed by an increase of the yield point (Fig. 1) as a MWCNT concentration increased (Fig. 2).

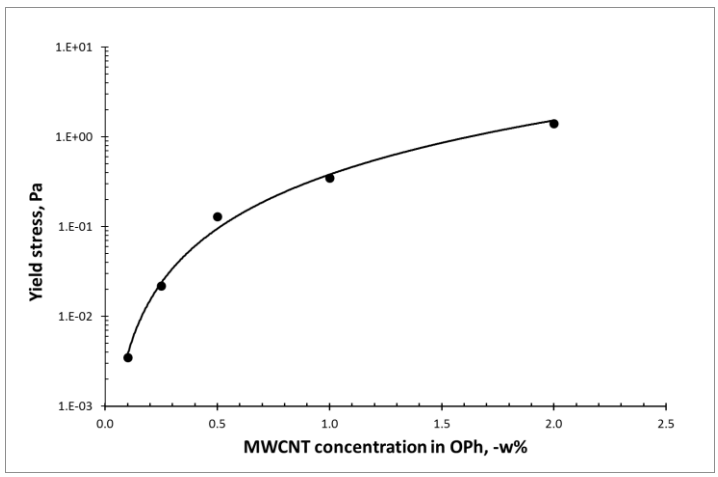

Figure 2 Effect of MWCNT concentration in oil on the yield stress of the oil phase

The second aspect of the study is the properties of emuslions as a function of MWCNT concnetration. By concentrating at the interface layer nanotubes play the role of an emulsion stabilizer (Fig. 3). But Fig. 4 shows that the presence of MWCNT does not affect the rheology of final emulsions. Similar resuts were obtained for pristine, -OH and –COOH functionalized MWCNT.

It is clearly seen (Fig. 4) that the yield stress as well as the plateau modulus of emulsions stabilized with MWCNT as a co-surfactant only slightly exceeds the same parameters of the emulsions stabilized without nano-tubes.

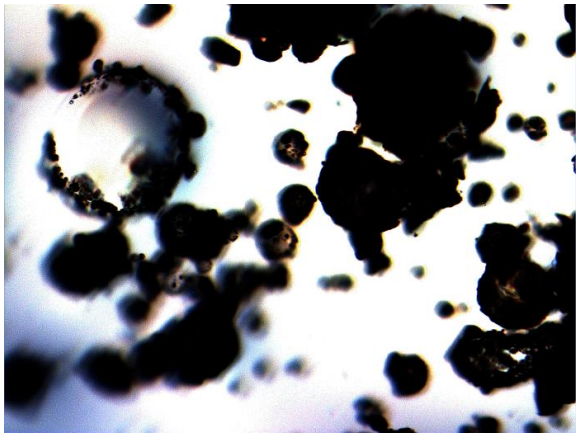

Figure 3 Microscopic image presenting the assembling of MWCNT at the droplets' interface

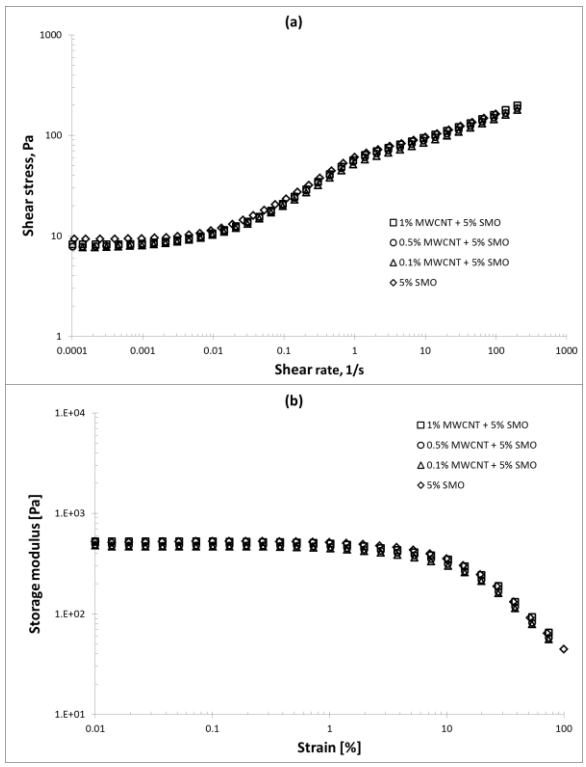

Figure 4. Rheological properties for 94% emulsions stabilized with 5% of SMO and different concentration of nanotubes: (a) shear stress vs. shear rate data; (b) storage modulus amplitude dependence at constant frequency 1 Hz.

Stability

The last, but not least, apect of the study is the stability of the emulsion. As was mentioned above the dispersed droplets are a super-cooled water solution of an inorganic salt which are prone to crystallization during ageing. So, all stability aspects are associated with the crystallization of the drops.

It was found that the MWCNT solely can stabilize our water-in-oil emulsion, but it is possible up to certain concentrations of the aqueous phase, which are rather low (see

Fig. 5). The use of pristine or –OH treated MWCNT does not affect the inversion point of w/o emulsion. At concentrations higher than 1% the inversion point drops. The MWCNT treatment probably promotes the formation of nanotube clusters in the oil phase which decreases the efficiency of stabilization. Moreover the emulsions are not stable against shearing.

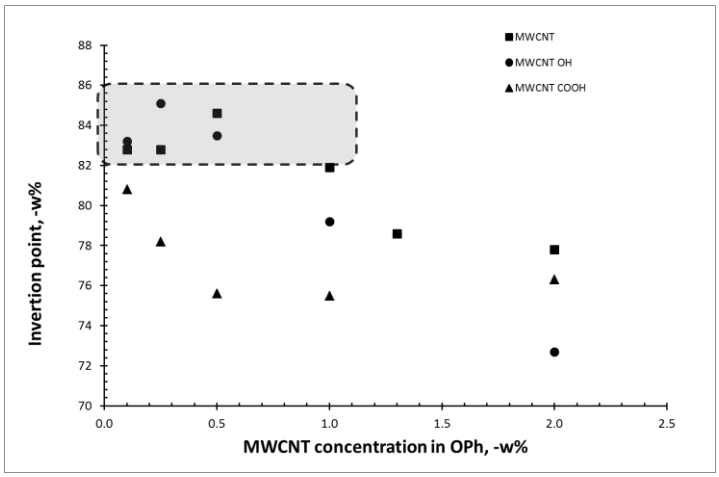

Figure 5. Inversion point (maximal aqueous phase concentration, -w%) of w/o emulsions as a function of the nanotube concentration in oil phase, emulsions stabilized by MWCNT solely.

A higher aqueous phase mass fraction and stability to shear can be achieved when MWCNTs are used as co-surfactant to classic surfactants such as SMO.
The data presented in Table 1 shows the effect of MWCNT concentration on the stability of highly concnetrated water-in-oil emulsions. The best stability (the best tehnological properties) was reached with the system containing 2% of pristine MWCNT and 5% of SMO in the oil phase or at 0.12% of nanotubes in the emulsion.

Table 1 Stability of emulsions stabilized by complex stabilizer: nanotubes and SMO

MWCNT treatment type	**Concentration of MWCNT in oil phase, % by weight**	**Ageing period before crystallization appears, days**
Pristine	0.1	< 45
	0.5	< 45
	1.0	< 45
	2.0	60
-OH	0.1	~ 30
	0.5	~ 30
	1.0	~ 30
-COOH	0.1	~ 30
	0.5	~ 30
	1.0	~ 30

CONCLUSION

Multiwalled carbon nanotubes can be used as emulsion stabilizers. The degree of MWCNT dispersion in the oil phase is important. The emulsion inversion point depends on the type of nano-tube treatment. Highly concentrted water-in-oil emulsions can be formed and are stable only when the MWCNTs are used in combination wuth the conventional surfactant such as SMO.

REFERENCES

1. Kong, J., Franklin, N. R., Zhou, C. W., Chapline, M. G., Peng, S., Cho, K. J. and Dai, H. J. (2000) Science, 287: 622.
2. Collins, P. G., Bradley, K., Ishigami, M. and Zettl, A. (2000) Science, 287: 1801.
3. Binks, B.P. and Lumsdon, S.O., (2001) Langmuir, 17: 4540-4547.
4. Binks, B.P. (2002) Curr. Opinion in Coll. Interface Sci., 7: 21-41.
5. Liu, X., Yi, Ch., Zhu Ye, Yang, Y., Jiang, J., Cui, Zh., Jiang, M., (2010) J. Coll. Interface Sci., 351: 315–322.
6. Matsui, J., Yamamoto, K., Miyashita, T. (2009) Carbon, 7: 1444 –1450.
7. Chen, Q., Saltiel, C., Manickavasagam, S., Schadler, L.S., Siegel, R.W., Yang, H. (2004) J. Coll. and Interface Sci., 280: 91–97.
8. Masalova, I., Malkin, A.Ya. (2008) Colloid J. 70 (3): 362-371.
9. Foudazi, R., Masalov, I., Malkin, A.Ya. (2010) Colloid J., 72 (1): 74-92.
10. Masalova, I., Foudazi, R., Malkin, A.Ya. (2011) Colloids and Surfaces A: Physicochem. Eng. Aspects, 375: 76–86.
11. Malkin, A.Ya., Masalova, I., Slatter, P., Wilson, K. (2004) Rheol. Acta, 43 (6): 584-591.
12. Masalova, I., Taylor, M., Kharatiyan, E., Malkin, A. Ya. (2005) J. Rheol., 49 (4): 839-849.

ACKNOWLEDGEMENT

The authors would like to gratefully acknowledge AEL Mining Services, the company which provided the financial support and permission to publish the results of these studies. We also thank Lake International Co. for supporting us with the classic surfactant.

USING FUMED SILICA NANO PARTICLES IN COMBINATION WITH SMO CONVENTIONAL SURFACTANT TO STABILIZE W/O HIGHLY CONCENTRATED EMULSION (EXPLOSIVE TYPE): EFFECT OF PARTICLE HYDROPHOBICITY ON RHEOLOGICAL PROPERTIES

*Nsenda Tshilumbu, *Masalova Irina

* Research Rheology Laboratory, Engineering Faculty, Cape Peninsula University of Technology,
PO Box 652, Cape Town, South Africa.

*Corresponding author: Masalovai@cput.ac.za

INTRODUCTION

Bulk emulsion explosives are progressively penetrating the underground mining market. They are replacing packaged explosives for reasons of improved safety, more efficient logistics, and high rates of detonation and reduced overall blasting costs [1]. The selection of the emulsifier that is used to prepare an emulsion explosive is of major importance. The emulsifier directly contributes to the ease of emulsion formation, the discontinuous phase droplet size and the emulsion stability and pumbability [2].

Most current commercial emulsion explosives make use of coventional surfactants such as PIBSA-based emulsifiers (PolyIsobutenyl Succinic Anhydride) or Sorbitan MonoOleate (SMO) to stabilize the oxidizer-fuel interface. Lots of research have been done related to the study of conventional surfactants. In the past two decades it became possible to produce solid particles in nano scale <100nm and to use them as emulsifiers to stabilize emulsion systems. These particulate stabilizers offer a number of advantages over conventional surfactants such as imparting improved stability against coalescence by providing a steric barrier at the interface and changing rheological properties of the emulsions [3-5]. However there are a few disadvantages: Polyhedral emulsions (HCE) stabilized by solid particles are highly sensitive to mechanical action and may become unstable under shear; it is difficult to manufacture highly concentrated W/O emulsions especially with the presence of inorganic salt in the dispersed phase; and no systematic study have been done in using the combination of nano- particles/conventional surfactants mixtures for stabilising W/O emulsions especially containing solution of salt as dispersed phase. The overall aim of this study is to determine how the particle hydrophobicity affects the physical structure (thin film network, and the structure at the interface oil-water) of fresh highly concentrated explosive emulsion, in mixture with SMO conventional surfactant.

MATERIALS AND METHODS

Continuous phase: A series of five fumed nanosilica dispersed in hydrocarbon oil were used for this study; 6wt% of each fumed nanosilica was mixed with 5wt% of a low molecular weight conventional surfactant sorbitan monooleate (SMO). The hydrophobicity index (HI) of particles used in this investigation were in the ranges: 0.60- 1.34 and HI > 3.
Dispersed phase: An aqueous solution of ammonium nitrate (AN). Water comprises < 20% by mass of the solution. Φ = 90vol%.
Droplet size distribution: The droplet size distribution was measured using the Malvern Mastersize 2000 technique.
Bottle test : A rapid indication on oil aggregation properties of particle dispersions in oil was given by the bottle test method by monitoring the extent of flow five minutes after the bottle has been fully inverted.
Interfacial characterisation and CMC: The dynamic interfacial tension were determined using a PAT 1 tensiometer supplied by Sinterface Technologies, Berlin.
Rheological characterisation: *All rheolo-gical measurements were carried out by using a rotational dynamic rheometer MCR 300 (Paar Physica).*

RESULTS AND DISCUSSIONS

Bottle test for particle dispersions in oil

Macroscopic considerations show that fumed silica particles behave as thickening agents of paraffin oil. For more hydrophilic particles (HI = 0.60 -0.72) the bottles fully inverted showed no flow (Fig.1a).
Addition of 5 wt% SMO destroys the 3D network structure: by adsorbing at the fumed silica nanoparticle surface, SMO decrease their gelling ability as evidenced in Fig.1b.

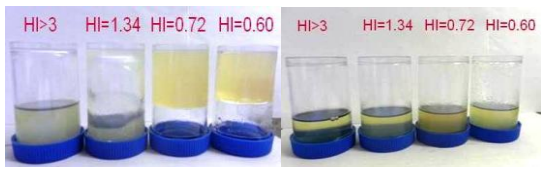

(a) **(b)**

Figure1: Photograph of 6wt % particles dispersion in oil (a) and mixture of 6wt% particles and 5wt% SMO in oil (b) 5 min after inverting the vessels.

Interfacial properties and CMC

To better understand the contribution of each species, SMO or fumed silica, in emulsions stabilized by the mixed emulsifier, interfacial and aggregation properties were determined (Table 1-3).

Table 1 Interfacial tension for different fumed silica, interfacial tension, Critical Micelle Concentration (CMC), Area per Molecule at the cmc (A_{cmc}) for SMO

Emulsifier	σ, mN/m	A_{CMC}, $Å^2$	CMC, mol/l
None	19.2	-	-
6% Fumed nanosilica	19.4	-	-
5% SMO	0.6	80	$0.6x10^{-4}$

Table 2 Radius of particles or aggregates (R) and estimated contact angle (Θ) for 100% coverage with dimethyl dichlorosilane [5].

Emulsifier	R, nm	Θ , degree
Fumed nanosilica, HI=1.34	12-50	164.2

The following points can be noted from Table 1 & Table 2:
The interfacial tension drops are significant in the presence of SMO compared to pure oil whereas in the presence of fumed nanosilica no interfacial tension effect is observed. This can be explained by the fact that the interactions between oil and water molecules are not modified by the presence of particles at the interface: on the contrary to the surfactant, particles do not replace molecules of water and oil at the interface, as these molecules adsorb into the porous structure of the particles [8].
The attachment energies of SMO and fumed nanosilica at the W/O interface can be estimated:

$$\Delta G°_{smo} = RT\ln(cmc) - (\sigma_o - \sigma)A_{cmc} \quad [1]$$

$$\Delta G_{part.} = \pi R^2 \sigma (1+\cos\Theta)^2 \quad [2]$$

Table 3 Attachment energies of SMO and fumed nanosilica at the W/O interface, in k_BT units.

% Silica (HI=1.34)	% SMO	ΔG_{SMO}	$\Delta G_{part.}$
6	0	-	16662.78 k_BT
0	5	15.75 k_BT	-
6	5	-	1.63 k_BT

It can clearly be seen from Table 3 that at 5wt% in the oil, SMO is able to replace fumed silica from the W/O interface [6-7]. This can be explained by the low value of the interfacial tension in the presence of SMO and the increase in particle contact angle due to the adsorption of SMO onto the fumed silica surface.

It seems reasonable to assume that when the mixed emulsifier system (SMO/particles) is used, only SMO adsorbs at the W/O interface for the following reasons:

- SMO molecules reach the W/O interface much quicker than fumed silica particles due to their lower molecular weight.
- The low attachment energy of nano-particles in the presence of SMO makes it difficult to replace SMO from the W/O interface.

Droplet size distribution

The size distribution of emulsion droplets immediately after preparation are shown in Fig. 2.

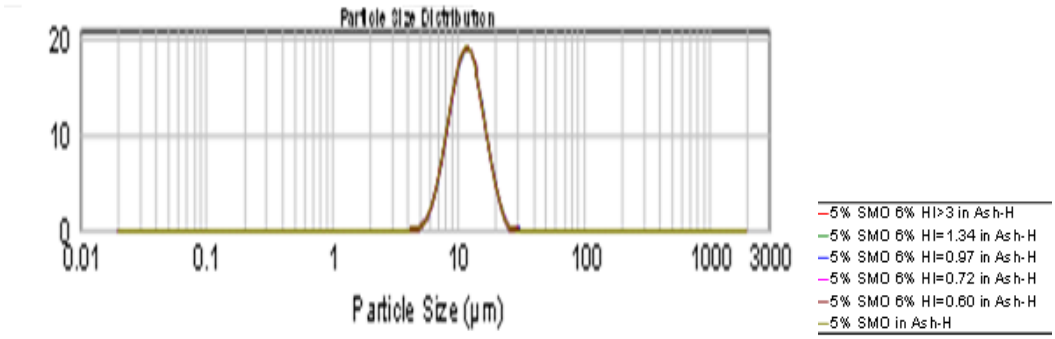

Figure 2 Histogram of drop size distribution of the emulsion for different HI

From the above it can be clearly seen that all samples had the same droplet size (10µm) and similar droplet droplet size distributions.

EFFECT OF HYDROPHOBICITY INDEX ON FLOW PROPERTIES OF EMULSION EXPLOSIVES

Flow curves and yield stress obtained for emulsions stabilized with 5wt% SMO and 6wt% of particles with different HI are shown in Fig. 3 and Table 4 respectively.
It is clear that the emulsions show a pronounced yield stress, but a hump in the flow curve at moderate shear rates (0.2- 0.6 s^{-1}) is seen Fig.3.

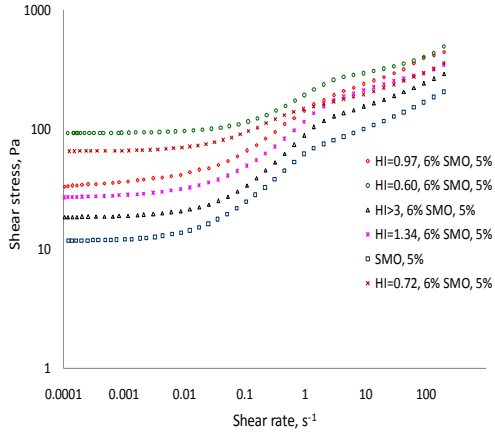

Figure 3 Flow curves for emulsions stabilized with 5wt% SMO and 6wt% of particles with different HI

This behaviour can be explained by Windhab's model [9] as a secondary yield stress. It was demonstrated that, at shear rates above the hump, the droplets are deformed during flow, while the rolling of droplets over each other is the dominant mechanism of flow at shear rates below the hump [10].

Table 4 Yield stress values for emulsions stabilized with 5wt% SMO and 6wt% of particles with different HI

SMO	HI>3	HI=1.34	HI=0.97	HI=0.72	HI=0.6
11.7	24.2	34	39	48.3	92

Table 4 shows that while the emulsion prepared with SMO alone has relatively low yield stress; the addition of fumed silica to the formulation significantly increases the magnitude of the yield stress. The effect of fumed silica on the yield stress of SMO based emulsion is amplified with reduction of HI. The yield stress of samples has the following trend: HI=0.60 > HI=0.72 > HI=0.97 > HI= 1.34 > (HI>3).
Treating the yield stress as the measure of the strength of a structure formed in emulsions, we can say that HI =0.60 provides the highest characteristics of a material. As evidenced by the bottle test for oil dispersions in the presence of 5wt% SMO, in all the above emulsions, the fumed silica network in the thin film between droplets is in a complete broken state. Moreover in all the above emulsions only SMO is expected to cover the interface (same interfacial properties). It can be concluded that the formation of a network of silica particles in the bulk phase and the interfacial tension or elasticity are not the only controlling parameters of flow behaviour.
One can calculate the amount of surfactant adsorbed on the dispersed droplets. The surface area per unit volume of droplets can be calculated as follows:

$$A_N = \frac{6\phi}{d_{32}} \qquad [3]$$

where Φ is the volume fraction of the dispersed phase. Therefore, based on the measured interfacial properties, about 0.65 wt % of SMO is enough to fully cover whole interfacial area for the emulsion with d_{32} = 10µm. Most of the surfactants remain in the oil phase adsorbed onto particles as is evident from adsorption tests [11] and form micelles as evident from Small Angle Neutron Scattering (SANS) studies

[12-14]. Keeping in mind that SANS results [12-14] revealed a spherical shape for SMO micelles with a mean radius of ca 22A^o and assuming an interdroplet thickness of 100nm [15], one can expect the presence of micelles in the interdroplet layer. The micelle content is expected to decrease with increase in surface density of OH groups (or decrease in HI). The exact reasons for the effect of HI are unclear and we can only make some suggestions. First, since it has been found that the dominant mechanism of flow at low shear rates for HCE is the rolling of droplets over each other [16], it can be assumed that the increase in the micelle concentrations with an increase in HI enhances this rolling mechanism due to the decrease in the friction between the interfacial layers. Secondely, it is well known that a fraction of micelles could become charged via a disproportionation process in which two neutral micelles interact to form one positively-charged and one negatively-charged micelle and that SMO micelles charges positively silica particles [17]. The strong electrostatic repulsion resulting from the above charges in the oil phase can be considered as a possible additional source of elasticity in liquid explosives. Thus, the higher concentration of micelles (i.e. higher HI) increases the possibility of charged micelles resulting in a decrease in the Debye length of electrostatic forces; and hence the electrostatic repulsion decreases. Less electrostatic repulsion leads to less storage of additional energy and resistance to flow.

EFFECT OF HYDROPHOBICITY INDEX ON VISCOELASTIC PROPERTIES OF EMULSION EXPLOSIVES.

Viscoelastic properties for emulsions stabilized with 5wt% SMO and 6wt% of particles with different HI are shown in Fig. 4-5.

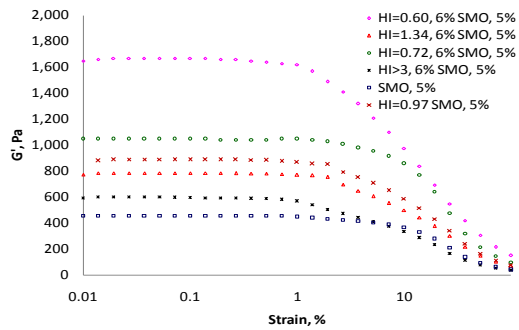

Figure 4 Effect of HI on viscoelastic properties

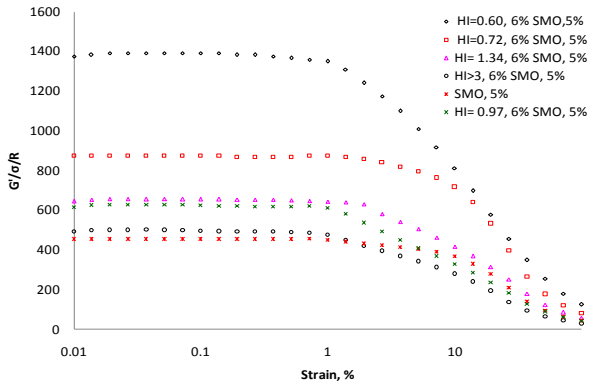

Figure 5 Effect of HI on the dimensionless elastic modulus

From the above observations, the following conclusions can be made:

Fig. 4 shows that the plateau modulus, G_p, pursues the same trend as for the yield stress: HI=0.60 > HI=0.72 > HI=0.97 > HI= 1.34 > (HI>3). It is clear that the scaling of storage modulus values by the Laplace pressure does not result in superimposition of the variations shown in Fig. 5. Again the significant effect of micelles is evident in this behaviour and possible mechanisms explained for flow behaviour and yield stress in the preceding section could be responsible, although the rolling mechanism of droplets over each other could not be present in the linear viscoelastic region due to the small amplitude oscillatory flow regime.

CONCLUSIONS

A series of five fumed silica types were used as emulsifiers to perform an investigation into the effect of the hydrophobicity index (HI) on the rheological properties of water-in-oil highly concentrated emulsions (HCE). The fumed nanosilica with different HI in the 0.60- 1.34 and HI> 3 range, were mixed with a low molecular weight conventional surfactant Sorbitan MonoOleate (SMO). The results obtained were compared to the properties of emulsions where only SMO act as the emulsifier. It was shown that addition of silica nanoparticles to SMO-based emulsions increases significantly all rheological parameters (yield stress and plateau modulus) of fresh emulsion. The effect was found to be more pronounced with decrease of HI. This is probably related to the reduction in micelle content with increase in HI due to a concomitant increase in the amount of SMO adsorbed onto the particle surface.

At low shear strain, the rheological properties of compressed emulsions under investigation seems to be sensitive to the micelle concentration. In this region of shear strain, deformation proceeds by larger droplets rolling over the smaller ones, and micelles acting as ball bearings (lubricants) between droplets. The higher the HI, the higher the expected micelle content and the less the elasticity appears to be.

NOMENCLATURE

ΔG_{part}	*attachment energy of particles at W/O interface*	*J*
ΔG_{smo}	*attachment energy of SMO at W/O interface*	*J*
σ	*interfacial tension*	*N/m*
R	*particle or aggregate radius*	*nm*
$k_B T$	*thermal energy*	*J*
Φ	*dispersed phase volume fraction*	

REFERENCES

1. Bampfield, H.A. & Cooper, J.1983. Encyclopedia of emulsion technology. Becher (ed.), Marcel Deker, New York, v.3.
2. Chattopadyay, A.K. 1966. US Patent, 5,500,062.
3. Arditty, S., Schmitt, V., Lequeux, F. & Leal-Calderon, F. 2005. Interfacial properties in solid-stabilized emulsions. *Eur. Phys. J. B, 4(3): 381-393.*
4. Aveyard, R., Binks, B.P. & Clint, J.H. 2003. Emulsions stabilised solely by colloidal particles. *Advances in Colloid and Interface Science* 100–102: 503–5462.
5. Binks, B.P. & Clint, J.H. 2002. Solid Wettability from Surface Energy Components:
Relevance to Pickering Emulsions. *Langmuir:* 18: 1270-1273.
6. Drelich, A., Gomez, F., Clausse, D. & Pezron, I. 2010. Evolution of water-in-oil emulsions stabilized with solid particles. Influence of added emulsifier *Colloids Surf. A* 365: 171.
7. Reynolds, P.A., Henderson, M.J., Zank, J. & White, J.W. 2011. Complex layering observed in high internal phase emulsions at a silicon surface
by neutron reflectometry. *J. Colloid and Interface Science* 364: 539–545.
8. Pichot, R., Spyropoulos, F. & Norton, IT. 2012. Competitive adsorption of surfactants and hydrophilic silica particles at the oil–water interface: Interfacial tension and contact angle studies. *J. Colloid and Interface Science* 377: 396–405.
9. Windhab, E. 1993. Bericht: IV. Tagung Lebensmittel rheologie detmold.
10. Masalova. I. & Malkin.Y.A. 2007. Shear and normal stresses in flow of highly concentrated emulsions. *J. Non-Newtonian Fluid Mech.* 147: 65–68.
11. Santhanalakshmi, J. & Balaji, S. 1996. Adsorption Studies of Nonionic Surfactants on Charcoal and Alumina in Aromatic Solvents. *J. colloid and interface science* 179: 517–521.
12. Reynolds, A.P., Gilbert, P.E. & White, W.J. 2000. High internal phase water-in-oil emulsions studied by small-angle-scattering. *J. Phys. Chem. B,* 104:7012–702.
13. Reynolds, P.A., Gilbert, P.E. & White, W.J. 2001. High Internal Phase Water-in-Oil Emulsions and related Microemulsions Studied by Small Angle Neutron Scattering. *J. Phys. Chem. B,* 105:6925–6932.
14. Reynolds, P.A., Zank, J., Jackson, A.J., Baranyai, K.J., Perriman, A.W., Barker, J.G. & White, W.J. 2006. Aggregation in a high internal phase emulsion observed by SANS and USANS. *Physica B* 385–386:776–779.
15. Masalova. I. & Malkin.Y. A. 2007. Rheology of Highly Concentrated Emulsions – Concentration and
Droplet Size Dependencies. *Appl. Rheol.* 17(42250): 1 – 9.

16. Masalova, I., Malkin, A. Ya, Ferg, E., Taylor, M., Kharatiyan, E. & Haldenwang, R. 2006. Evolution of rheological properties of highly concentrated emulsions with aging—Emulsion-to-suspension transition. *J. Rheol.*, 50(4):435–451.
17. Poovarodom, S. & John, C. B. 2010. Effect of particle and surfactant acid–base properties on charging of colloids in apolar media. *J. Colloid and Interface Science* 346: 370–377.

RHEOLOGY OF MAIZE STARCH MODIFIED WITH LIPIDS

MN Emmambux, OC Wokadala

Department of Food Science, University of Pretoria, email: naushad.emmambux@up.ac.za

INTRODUCTION

Starch is widely used as an ingredient to improve the texture of various processed foods due to the viscous properties of its pastes. Starch can be modified with naturally occurring lipids for example stearic acid to produce high viscosity pastes. For example, during biphasic starch pasting, the paste viscosity of maize starch after prolonged pasting can be up to three times that of the commonly observed paste viscosity after pasting for a short time (D'Silva et al., 2011). This paper determines the rheology (pasting and viscoelastic properties) of maize starches modified with stearic acid during pasting.

MATERIAL AND METHODS

RAW MATERIALS

Teff Starch was extracted from South African white teff (Witkop, Pannar, Kroonstad, South Africa) according to the method used by D'Silva et al., (2011). Commercial white normal maize starch (Amyral©) was obtained from Tongaat Hulett (Edenvale, South Africa).

METHODS

Starch pasting using the RVA

A rapid visco analyzer unit (RVA, Model 3D, Newport Scientific-Warriewood, Australia) was used for pasting and to record viscosity. Stearic acid was incorporated into the starch according to D'Silva et al., (2011) at 1.5% w/w of the starch (dry basis). This stearic acid level was also shown to give a high and optimal second biphasic paste viscosity (D'Silva et al., 2011). The defatted maize starch (10% w/w) with or without added stearic acid was pasted for up to 130 min. The RVA conditions were 960 rpm and 50 ºC for 10 sec, then heated to 90 ºC at a rate of 10 °C/min with 160 rpm stirring, then held constant for the required time.

Differential scanning calorimetry

The thermal properties of the freeze dried pastes were assessed using a high pressure DSC system with STARe® software (HPDSC-827, Mettler Toledo, Greifensee, Switzerland). Analyses were conducted on both freeze dried teff and maize starch pastes obtained after pasting for 130 min. The starch powder (10 mg) was mixed with

distilled water (30 mg), and then equilibrated for at least 2 h at room temperature. Scanning was done from 40 to 125 °C at a rate of 10°C/ min. Indium (Tp = 156.61 °C, 28.45 J/g) was used as a calibration standard for the DSC with an empty pan as a reference.

Rheological analysis

An MCR 101 (Anton Paar GmbH, Austria) rheometer was used to determine the viscoelastic properties of the starch paste during a temperature followed by a time sweep to simulate the storage conditions. The LVE range was first determined. The paste was cooled from 91 °C to 4 °C and maintained at this temperature for 5 hours. The strain was 0.5% and the frequency was at 1rad/sec. A plate-plate configuration was used.

RESULTS AND DISCUSSION

Two paste peak viscosities (biphasic pasting) were observed when maize starches with added stearic acid were pasted for a prolonged time (130 min) (see Fig. 1). The maize starch pasted without added stearic acid showed a small paste peak viscosity at about 30–60 min of pasting and the viscosity also decreased with prolonged pasting time (see Fig. 1). Maize starch pasted with added stearic acid had a paste viscosity of about 361.0 RVU after prolonged pasting while that pasted without added stearic acid had a viscosity of about 83.0 RVU.

The modified starches that have a very high paste viscosity showed an endotherm at about 100-120 °C (Fig. 2). This endotherm has been characterised as type II amylose lipid complexes (Biliaderis et al., 1986; Raphaelides & Karkalas, 1988). These are supra structures of a high molecular order.

During cooling of maize starch, the G´ and complex viscosity increase rapidly compared with the paste modified with stearic acid. The paste modified with stearic acid seems to maintain the same complex viscosity and the elastic modulus. This is important and it seems that the modified starches do not gel during cooling and storage at low temperature. The non-gelling nature may be due to limited junction zone formation and double helix formation of amylose to reduce retrogradation (D'Silva et al, 2011)). Retro gradation of starches is a major drawback in starch utilisation.

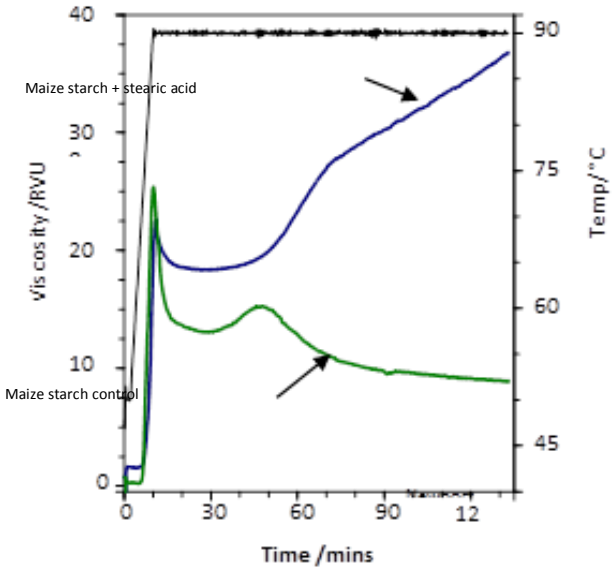

Figure 1 Effect of stearic acid addition on the pasting properties of maize starch

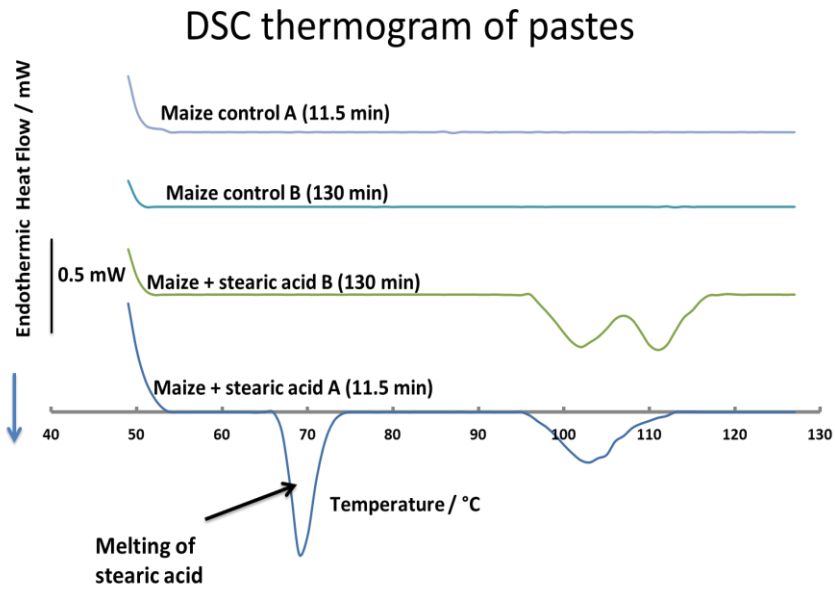

Figure 2 Effect of stearic acid addition on the thermal properties of maize starch after pasting

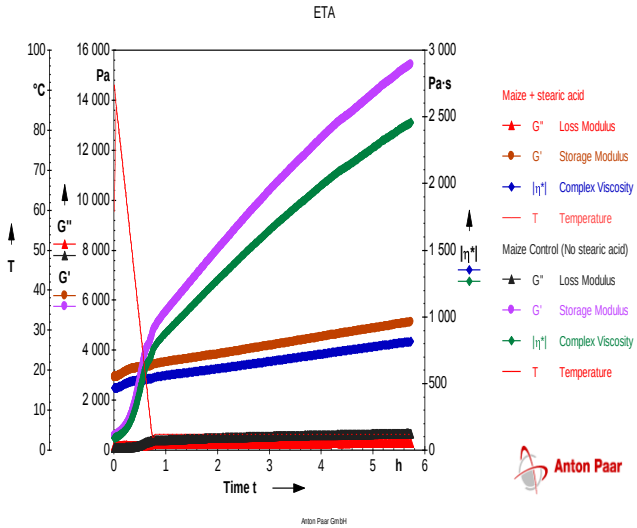

Figure 3 Effect of stearic acid addition on the viscoelastic properties of starch paste during cooling temperature and time sweep.

CONCLUSIONS

During extended pasting of maize starch with stearic acid, amylose lipid complexes play an important role in producing the high peak viscosity. The modified starches are non-gelling and have potential application as non-gelling starches for example in pies and as thickeners in soups and other.

REFERENCES

1. D'Silva, T. V., Taylor, J. R. N, Emmambux, M. N. (2011). Enhancement of pasting properties of teff and maize starches through wet-heat processing with added stearic acid. *Journal of Cereal Science*, *53* 192-197
2. Biliaderis., C. G., Page, C. M., Maurice, T. J. (1986). Non-equilibrium melting of amylose-V complexes. *Carbohydrate Polymers, 6*, 269-288.
3. Raphaelides, S., Karkalas, J. (1988). Thermal dissociation of amylose-fatty acid complexes. *Carbohydrate Research, 172*, 65-82.

METHODOLOGY FOR COUPLED CFD-DEM MODELLING OF PARTICULATE SUSPENSION RHEOLOGY

Smuts, EM*, Deglon, DA*, Meyer, CJ°

*Minerals to Metals, Chemical Engineering Department, University of Cape Town, Rondebosch, Cape Town, 7701, E-mail: evan.smuts@gmail.com
*Minerals to Metals, Chemical Engineering Department, University of Cape Town, Rondebosch, Cape Town, 7701, E-mail: david.deglon@uct.ac.za
°Department of Mechanical and Mechatronic Engineering, Stellenbosch University, Private Bag X1, Matieland, 7602, E-mail: cjmeyer@sun.ac.za

INTRODUCTION

This paper describes a methodology used to develop a numerical model for the study of particulate suspension rheology. The methodology was first validated with Computational Fluid Dynamics (CFD) models for both a Newtonian fluid (water), and a non-Newtonian Herschel-Bulkley slurry in rheometers of different geometries. Rheograms have been reproduced from these models and compared to experimental values.

A combination of CFD and the Discrete Element Method (DEM) was then used to create a model of the particle-fluid system. CFD uses a continuum approach to model the fluid component, which is a fast and computationally efficient method. DEM on the other hand resolves the behaviour of each individual particle, which accounts for the individual nature of the contact and non-contact forces between particles.

Because CFD and DEM are very different in their modelling approach, two separate software programmes were used. For CFD, OpenFOAM® [1] was chosen, and for the DEM, a programme called LIGGGHTS [2] was used. Both of these packages are freely available as open source codes written in C++ and allow for the addition of custom code through user-created libraries. The developers of LIGGGHTS have already written code called CFDEM [3] that can couple, or share information between, the two programmes.

This coupled model is currently capable of modelling spherical particles in a suspending liquid. The DLVO force has been included in some models to account for inter-particle forces due to the surface charge on the particles. This force, originally proposed by Derjaguin and Landau [4] and Verwey and Overbeek [5], is a combination of the van der Waals and electrostatic double layer forces. The coupled model is currently being validated. Preliminary results for plain particles (no DLVO forces) show good qualitative behaviour of the model. With this model, particle properties such as size, shape and surface charge can be studied to determine their overall effect on suspension rheology.

CFD MODEL

The first phase of the methodology was the development of a CFD model of a rheometer to test the performance of CFD against experimental data. Torque on all moving (rotating) boundaries was calculated and converted to a shear stress value.
In CFD, the fluid phase is assumed to be a continuum, and the Navier-Stokes equations are used to describe the fluid flow. It is assumed that the flow follows Couette flow, where the flow is laminar and incompressible. In addition, the flow is also time-dependant due to the varying shear rate which occurs in controlled shear rate rheometers.

Model Description

A CFD mesh was created that mimicked the shape and behaviour of a rheometer. The simplest design is a single-gap rheometer which consists of one set of concentric cylinders. An adaptation of the single gap rheometer is the DIN bob, which has a conical tip to limit the influence of end effects. DIN is the Deutsches Institut für Normung, which in English, is the German Institute for Standardization.
In all cases, a thin slice of the full geometry was modelled, reducing the model size, and as a result, the computational expense. For the single and double gap, a horizontal slice was modelled as it was assumed that the end effect would be negligible when compared to the full length of the rheometer.

Newtonian Fluid Results

Water was selected for the Newtonian fluid as a benchmark fluid because most slurries contain water. The performance of the model was judged as to how close it could match the value for water's dynamic viscosity.
Both the single and double-gap geometries performed well at slower shear rate changes and smaller gap widths, with viscosity values within one percent of experimental viscosity. One important observation is the large difference between the performance of the DIN bob geometry and the other two. While both the single and double gap geometry are very accurate, the DIN bob does not even achieve a reasonable experimental error (10 – 50%). This is most likely due to the end effects that are present in the DIN bob model (the ends of the single and double-gap models were not modelled).

Non-Newtonian Fluid Results

It was decided to also simulate a non-Newtonian fluid as most suspensions are non-Newtonian. A mineral slurry containing a vermiculite-quartz mix was selected [6]. Only the single-gap and DIN bob geometries were tested. Similarly with the Newtonian case, a good correlation was found between the fitted Herschel-Bulkley model and the CFD results. The DIN bob performed much better in this case, but it still deviated slightly at higher shear rates. This shows the model is able to handle fluids that are more complex than simple Newtonian liquids.

DEM MODEL

DEM uses Newton's Second Law of Motion to calculate the resultant trajectories (position and motion) of each particle from the different forces acting on them (e.g. fluid drag, or electrostatic forces). Particles forces that were considered are:

- Particle-particle contact - for computational efficiency reasons, the linear Hooke model was chosen for inter-particle collisions.
- DLVO interaction force - modelled to account for non-contact attraction and repulsion forces between particles [4, 5].
- Fluid-particle drag force - this force is the means by which the fluid imparts motion onto particles. Di Felice's drag model was employed [7].

COUPLED CFD-DEM MODEL

A number of practical factors had to be considered for the design of the coupled model. Computational efficiency had to be considered during model sizing.

Governing Equations for Coupled Flow

The fluid phase equations have to be altered to include the effects of momentum transfer due to particles suspended within the fluid. Most literature on fluid-particle systems mentions two different formulations of the fluid flow equations that are commonly used, namely Model A and Model B (e.g. [8]; [9]). However, based on the analysis of [10], Model A would be more suitable for this system.
A pair of governing equations are used to decribe the fluid phase. The first, which decribes the conservation of momentum, is given by

$$\frac{\partial(\varepsilon_f)}{\partial t} + \nabla \cdot (\varepsilon_f \boldsymbol{u}_f) = 0$$

and the second decribes the conservation of mass:

$$\frac{\partial(\rho_f \varepsilon_f \boldsymbol{u}_f)}{\partial t} + \nabla \cdot (\rho_f \varepsilon_f \boldsymbol{u}_f \boldsymbol{u}_f) = -\varepsilon_f \nabla p - \boldsymbol{F}_{pf}^{A} + \varepsilon_f \nabla \cdot \boldsymbol{\tau} + \rho_f \varepsilon_f \boldsymbol{g}$$

Here $\boldsymbol{F}_{pf}^{A}$ is the volumetric particle-fluid interaction force, $\boldsymbol{u}_f$ is velocity, p is pressure, $\boldsymbol{\tau}$ is the stress tensor, and ε_f is the fluid volume fraction. The particle-fluid interaction force for Model A is made up of the particle drag force, the pressure gradient force, and the viscous force due to fluid shear stress.

Model Geometry and Boundary Conditions

In order to take advantage of LIGGGHTS' limited ability to handle periodic boundaries, it was decided to restructure the circular CFD domains into a flat-edged

box. This is equivalent to unravelling the circular ring of the single-gap rheometer into a linear domain with one wall translating past the other. To further reduce the number of particles required, a smaller domain size was also used. The lower limit of the box size is still under investigation, but the current size is a cube with sides of 50 μm in length. The cell size of the hexagonal mesh is roughly 4.2 particle diameters in each direction.

Time Step Size and Coupling Procedure

Due to the physics involved in many coupled systems, the DEM time step generally needs to be much smaller than the CFD time step. The time step has to be sufficiently small to capture the energy transmission by wave propagation [11]. To establish the upper limit of the DEM time step, the criteria of the Rayleigh time was used, as it is typically suited to dense systems. The Rayleigh time is the time taken by the Rayleigh surface wave to propagate through a solid particle. It is defined as

$$dt_R = \frac{\pi r \sqrt{\rho_p / G}}{(0.1631\nu + 0.8766)}$$

where r is the particle radius, ρ_p is the particle density, G is the shear modulus, and ν is the Poisson's ratio.

CFDEM runs the CFD and DEM solvers concurrently. Because the CFD timestep is often much larger than the DEM timestep, the DEM solver runs for a number of timesteps before the information is transferred to the CFD solver, which usually only iterates for one timestep between coupling. The number of (DEM) timesteps between coupling events is known as the coupling interval, and is typically in the region of 50 – 100 timesteps.

Preliminary Validation of Coupled Model

In order to validate the coupled model, experimental data from [12] was used. Part of their work covers rheological data for spherical zirconia particles. They also include detailed data on the DLVO interaction forces which is useful in reconstructing the material parameters needed in the computer model. Using this experimental data, the model will be tested against different particle volume fractions. The shear rates will be increased from zero, up to 180 s^{-1}. However, final simulations have not been completed yet, and so only preliminary results are presented here.

Figure 4 compares initial coupled model results with experimental values for a particle volume fraction of 4.68% and pH of 4.5. CFD results for pure water are shown for comparison to illustrate the effect of adding particles to the model. Plain particles (no DLVO forces) significantly increase the shear stress. Including DLVO forces further increases the overall shear stress as expected, but didn't produce a sizeable increase in shear stress as the shear rate was increased. The electrostatic force was calculated for pH of 4.5, with a corresponding zeta potential of 32 mV. It should be noted that the experimental data were measured using a coaxial cylinder geometry, whereas the numerical results were calculated for a box-shaped domain. However, these geometries were found to be equivalent in pure CFD tests.

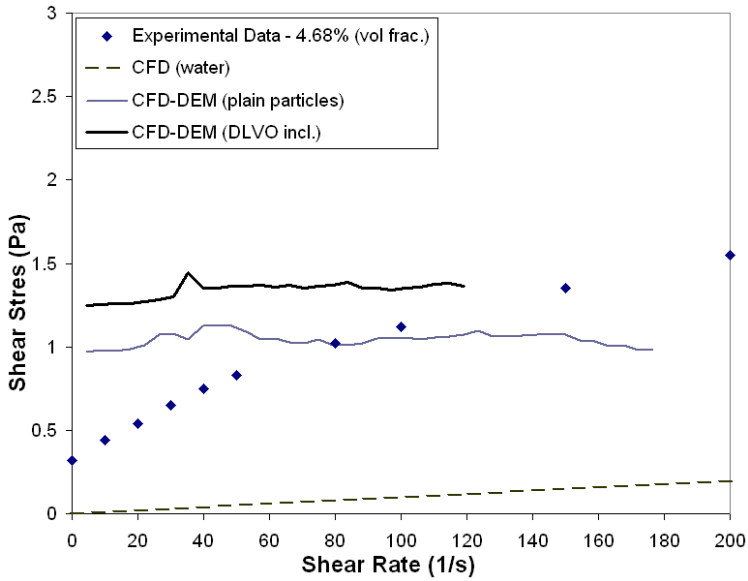

Figure 4 Rheogram comparing coupled model data with experimental values

CONCLUSIONS

The methodology for the development of a CFD-DEM numerical model for particulate suspensions has been described. At each major step in the development, testing has been done to assess its behaviour under different conditions. For the pure CFD model, the results were very good. Accurate representations of the known fluid behaviour for both Newtonian and non-Newtonian cases were achieved. While the coupled model does exhibit some good trends, work still needs to be done to refine it further.

REFERENCES

1. Weller, H.G. Tabor, G., Jasak, H., & Fureby, C. 1998. A tensorial approach to computational continuum mechanics using object orientated techniques, *Computers in Physics*, 12:620–631.
2. Kloss, C. & Goniva, C. 2010. LIGGGHTS – A New Open Source Dem Simulation Software, in *5th International Conference on Discrete Element Methods (DEM5)*.
3. Goniva, C., Kloss, C., Hager, A. & Pirker, S. 2010. An Open Source CFD-DEM Perspective, in *Proceedings of OpenFOAM Workshop*, Göteborg.
4. Derjaguin, B.V., & Landau, L. 1941. Theory of the stability of strongly charged lyophobic sols and of the adhesion of strongly charged particles in solutions of electrolytes. *Acta Physicochem*, 14:633–662.
5. Verwey, E.J.W., & Overbeek, J.T.G. 1948. Theory of the stability of lyophobic colloids - The interaction of soil particle having an electrical double layer. Amsterdam. Elsevier.
6. Ndlovu, B., Becker, M., Forbes, E., Deglon, D. & Franzidis, J.P. 2011. The influence of phyllosilicate mineralogy on the rheology of mineral suspensions, *Minerals Engineering*, 24:1314-1322.

7. Di Felice, R. 1994. The voidage function for fluid–particle interaction systems, *International Journal of Multiphase Flow*, 20:153–159.
8. Zhu, H.P., Zhou, Z.Y., Yang, R.Y., & Yu, A.B. 2007. Discrete particle simulation of particulate systems: theoretical developments, *Chemical Engineering Science*, 62:3378-3396.
9. Feng, Y. & Yu, A. 2003. Numerical simulation of the gas-solid flow in a fluidized bed by combining discrete particle method with computational fluid dynamics, in *Third International Conference on CFD in the Minerals and Process Industries*, Melbourne, December 2003. 475-480.
10. Zhou, Z.Y. Kuang, S.B. Chu, K.W. & Yu, A.B. 2010. Discrete particle simulation of particle-fluid flow: model formulations and their applicability, *Journal of Fluid Mechanics*, 661:482-510.
11. Li, Y., Xu, Y. & Thornton, C. 2005. A comparison of discrete element simulations and experiments for 'sandpiles' composed of spherical particles, *Powder Technology*, 160:219-228.
12. Megias-Alguacil, D., Duran, J.D.G. & Delgado, A.V. 2000. Yield stress of concentrated zirconia suspensions: correlation with particle interactions, *Journal of Colloid and Interface Science*, 231:74-83.

A COMPARISON OF 150 NB PIPELOOP DATA WITH ROTATIONAL VISCOMETER TEST METHODS

Brian Zengeni, Ros Malloch, Fritz van Sittert

Paterson & Cooke Consulting Engineers (Pty) Ltd, Cape Town, South Africa.
E-mail: BrianZ@PatersonCooke.com

INTRODUCTION

This paper presents a comparison of actual pressure loss data measured in a 150 NB pipeline to predictions estimated from conventional bob in cup (narrow gap) rotational viscometer data, "bob in an infinite cup" data and "vane in an infinite medium" data.

Data was recorded over a mass concentration range that varied from 61.3 %m to 69.4 %m that corresponds to Bingham yield stress values from 20 Pa to 150 Pa.

The viscometer data obtained using the three methods was analysed to obtain the Bingham yield stress and Bingham plastic viscosity of each sample. These parameters were used to calculate the equivalent wall shear stress and bulk shear rate in the test pipeline and compared to the measured data points on a pseudo shear diagram.

MATERIAL PROPERTIES OF MINERAL TAILINGS TESTED

The tests described in this section were conducted to determine the material properties of fine viscous mine tailings used for the test work. The results are summarised in Table 1.

Table 1 Mine material properties

Property Tested	**Mine Tailings**
Solids density	4324 kg/m^3
d_{90} particle size	79 µm
d_{50} particle size	17 µm
% passing 25 µm	55 %
% + 75 µm	11 %

Solids Density

The solids density of the slurry is measured using a helium pycnometer, which determines the volume of the solids particles accurately by displacing the air between particles with helium in a fixed volume cell.

Particle Size Distribution

The particle size distribution in Figure 1 is determined by a combination of dry sieving (+75 µm fraction) and hydrometer analysis (-75 µm fraction) according to the method detailed in ASTM D422-63 "Standard Test Method for Particle Size Analysis of Soils".

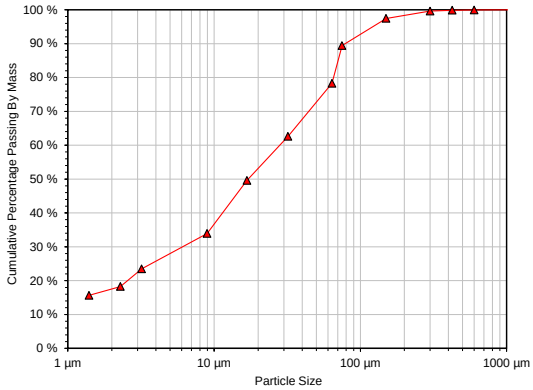

Figure 5 Particle size distribution

ROTATIONAL VISCOMETER TESTS

An Anton Paar Rheolab QC rotational viscometer was used to determine the viscous properties of the slurry over the range of concentrations tested. Tests were conducted using fully sheared slurry, i.e. the slurry was thoroughly mixed by the pump in the pipe loop and there was no reduction in yield stress on further shearing with a hand mixer, so the slurry was considered fully sheared. The data was analysed by applying the Bingham plastic model which is a two parameter model that describes the laminar flow behaviour. The two parameters are the Bingham plastic viscosity (K_{BP}) and Bingham yield stress (τ_{yB}).

The form of the Bingham plastic model is as follows:

$$\tau = \tau_{yB} + K_{BP}\gamma \qquad (1)$$

where: τ = shear stress (Pa)

τ_{yB} = Bingham yield stress (Pa)

K_{BP} = Bingham plastic viscosity (Pa.s)

γ = shear rate (s^{-1}).

Conventional Bob in Cup Method

The Searle system is where the bob rotates and the cup is stationary [1]. The CC35/HR (measuring bob radius = 17.5 mm, measuring cup radius = 21.0 mm, gap length = 52.5 mm, cone angle 120 °) measuring system was selected for this work.

The rotational viscometer recorded the torque measured over a range of shear rates from 5 to 300 1/s. The measured values of torque and shaft speed were translated into wall shear stress and shear rate according to ISO 3219 standard procedures. All data was analysed to account for end effects and secondary flow.

Bob in an Infinite Cup Method

The CC35/HR measuring system bob is immersed in a beaker that is at least twice the diameter of the bob and twice the height of the bob. The rotational viscometer records the torque and speed measured over a range of shear rates from 5 to 300 1/s. The measured speed is converted to angular velocity (Ω) and the following basic equation for coaxial rotational viscometers considered:

$$\frac{d\Omega}{d\sigma_b} = \frac{f(\sigma_b)}{2\sigma_b} \qquad (2)$$

where: Ω = Angular velocity (rad/s)

σ_b = Shear stress at the bob (Pa).

Solving equation (2) for the shear rate at the bob and multiplying the numerator and denominator by Ω, and simplifying equation (2), the following equation is obtained that can be used to determine the shear rate at the bob in the infinite cup method [1]:

$$f(\sigma_b) = \gamma_b = (2\sigma_b)\frac{d\Omega}{d\sigma_b} = \left(\frac{2\Omega\sigma_b}{\Omega}\right)\frac{d(\Omega)}{d\sigma_b} = (2\Omega)\frac{d(\ln\Omega)}{d(\ln\sigma_b)} \qquad (3)$$

Vane in an Infinite Medium Method

The ST22-4V-40 (vane diameter = 20 mm, vane height = 40 mm) measuring system was used. The vane has been shown to behave as a solid cylinder when rotated in this way in a body of fluid [2]. Thus the method of calculating the shear stress and the shear rate at the bob is similar to that used in the bob in an infinite cup method in section 3.2 [3].

LARGE SCALE PIPE LOOP TESTS

The test loop used to determine the pressure gradients for the mine tailings consisted of a 150 NB pipe loop, with a clear viewing section, a variable speed centrifugal pump, instrumentation and a computer-based data acquisition system. A magnetic flow meter was used to measure the pipeline flow rate. Slurry densities were measured by direct sampling and confirmed by the actual measurement of the solids mass concentration after drying the samples in a laboratory oven.

Clear Water Test Results

The proper operation of the flow meter, differential pressure transducers and pressure tappings was confirmed by clear water tests before and after the slurry test series. Figure 6 presents the clear water test results before and after the test series for the 150

NB test pipeline. The average hydraulic roughness is calculated from the measured water test data points using the Colebrook-White friction factor and the Darcy equation. The average measured hydraulic roughness for the 150 NB carbon steel pipe (ID = 155.68 mm) is 5 µm. This is within the range expected for a smooth wall pipeline.

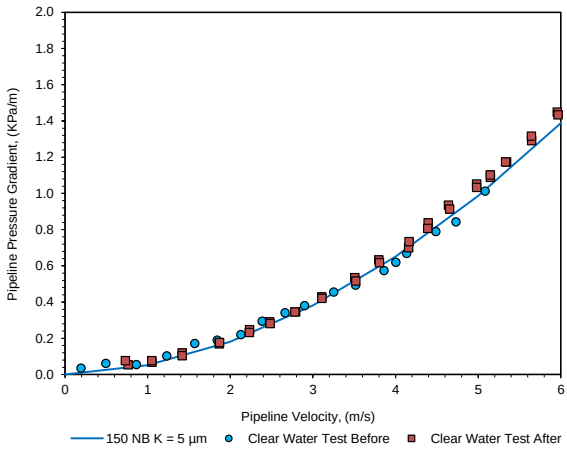

Figure 6 Clear water test results

TEST RESULTS

Pseudo Shear Diagram

The measured rheograms obtained from each set of viscometer data were analysed to obtain the best fit Bingham plastic parameters of yield stress and plastic viscosity.

In order to compare this data to the measured pipeline test data, all data was plotted on a pseudo shear diagram. A pseudo shear diagram is a plot of wall shear stress versus pseudo shear rate. The viscometer data was converted to a pseudo shear diagram using the Buckingham Equation. The Buckingham equation uses the Bingham plastic model parameters from equation (1) to convert the true shear rate to pseudo shear rate as follows [4]:

$$\frac{8V}{D} = \left(\frac{\tau}{K_{BP}}\right)\left[1 - \frac{4}{3}\left(\frac{\tau_{yB}}{\tau}\right) + \frac{1}{3}\left(\frac{\tau_{yB}}{\tau}\right)^4\right] \qquad (4)$$

where: V = Pipeline velocity (m/s)

D = Pipeline internal diameter (m).

Comparison of Data

Figures 4 to 7 show comparisons of the 150 NB pipe loop data with the different test methods performed using the rotational viscometer for varying solids concentrations. The yield stress varies from approxiamtely 150 Pa in Figure 4 to 30 Pa in Figure 7.

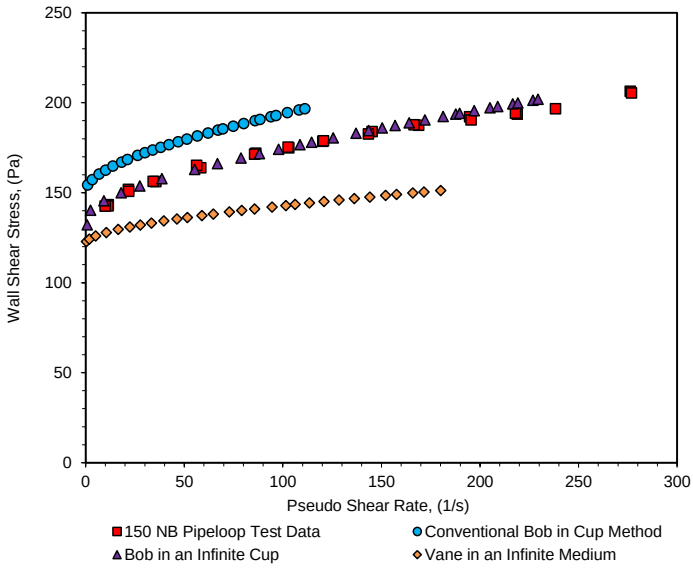

Figure 7 Comparison of 150 NB pipe loop data with rotational viscometer test methods at 69.4%m

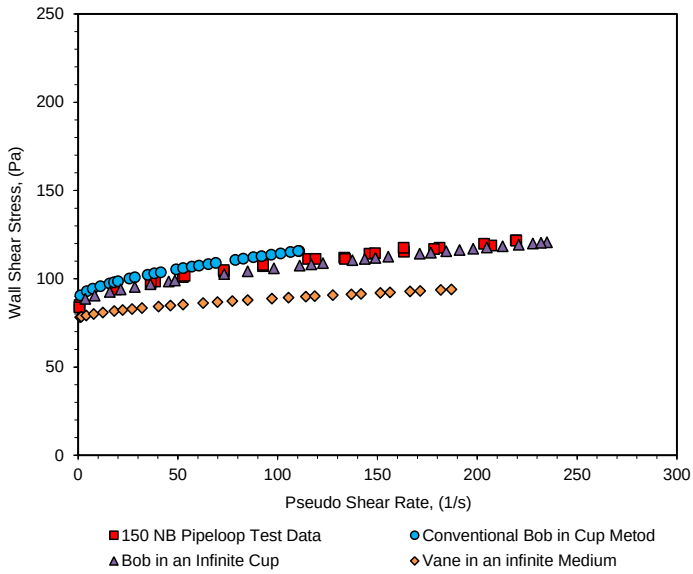

Figure 8 Comparison of 150 NB pipe loop data with rotational viscometer test methods at 67.1%m

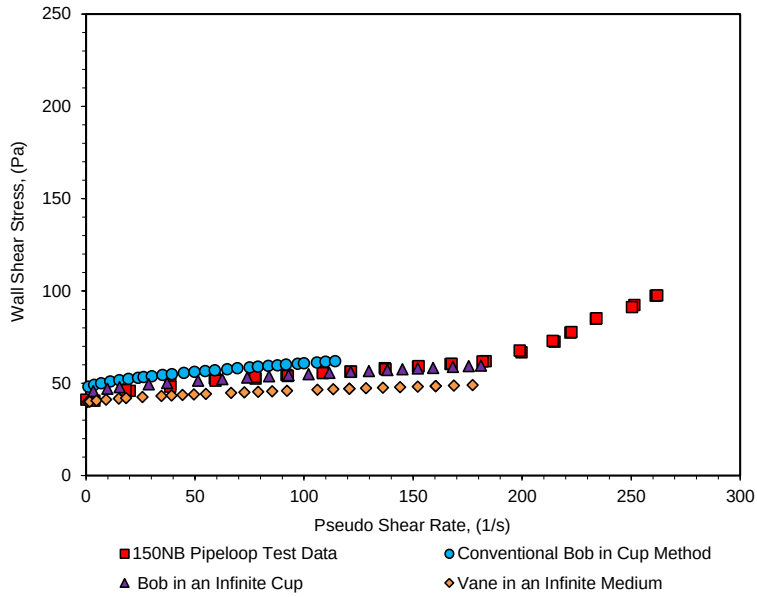

Figure 9 Comparison of 150 NB pipe loop data with rotational viscometer test methods at 65.3%m

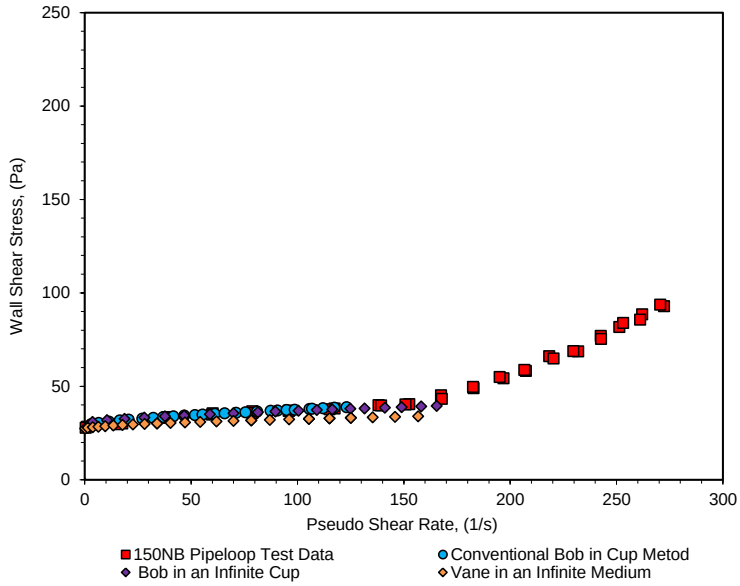

Figure 10 Comparison of 150 NB pipe loop data with rotational viscometer test methods at 61.3%m

CONCLUSION

It can be seen from the different rotational viscometer methods that the bob in an infinite cup data agreed best with the pipe loop data across the range of solids concentrations and yield stress values measured. The remaining rotational viscometer geometries tested did not give as good agreement with the pipe loop data.

As the yield stress decreases the accuracy of the conventional bob in cup (narrow gap) method improves and it better estimates the measured pipeline data. The vane in an infinite medium tended to under predict the shear stress for this type of slurry over the range of concentrations tested.

FUTURE WORK

This work showed that different rotational viscometer methods provide varying results and that they do not necessarily provide an accurate means to estimate large diameter pipeline pressure losses. Care needs to be taken when using rotational viscometer data to estimate pipeline pressure losses and a thorough understanding of the limitations and application of each method is needed.

REFERENCES

1. Steffe, J.F. 1996. *Rheological methods in food process engineering.* 2nd ed. East Lansing, USA: Freeman Press.
2. Barnes, H.A and Carnali, J.O. 1990. The vane in-cup as a novel rheometer geometry for shear thinning and thixotropic materials. *Journal of Rheology*, Vol. 34, No. 6:841–866.
3. Sofra, F, Fisher, D.T and Boger, D.V. 2007. The bucket rheometer for thickened tailings and paste flow curve determination. *10th International Seminar on Paste and Thickened Tailings*, Perth, Australia, Centre for Geometrics, Perth, March 2007:249-257.
4. Govier, G.W. and Charles, M.E. 1961. The hydraulics of pipeline flow of solid liquid mixtures, *75th E.I.C. Annual General Meeting*, Vancouver, Canada, May 1961.

NOTES

NOTES

NOTES

NOTES

NOTES